UNIVERSITE KASDI MERBAH OUARGLA

Faculté des Mathématiques et des Sciences de la Matière

Département de Physique

Mémoire

MASTER ACADEMIQUE

Domaine : Science de la Matière

Filière : Physique

Spécialité : Physique des Matériaux

Présenté par : Rihab LAKHAL & Fatima HARMA

Thème

Effet du dopage par NiO sur les propriétés microstructurales de la phase Bi2212

Soutenu publiquement

Le:17/06/2021

Devant le jury :

Mr. Nacer BOURAS	**MAA**	**Président**	**UKM Ouargla**
Mme. Karima BELAKROUM	**MCA**	**Encadrante/rapporteur**	**UKM Ouargla**
Mme. Mouna BATOUCHE	**MAA**	**Examinateur**	**UKM Ouargla**

Année Universitaire :2020/2021

Dedicate

This work is dedicated to the most expensive person in my heart: the most beautiful mother of all mothers "Safia", who has supported me in my life and gave me all to encourage, help and plant in myself the love of work and study and gave me an endless love,

To my dear father "Boufeldja" who encouraged me to have faith and the spirit of challenge and competition, I wish to be a doctor like him.

To my brothers for their support

To all my grandparents, may God have mercy on them,

To all my uncles.

To My sister and my beloved Rihab, the gift of God for me,

To all my friends.

FATIMA

Dedicate

This work is dedicated to the most expensive person in My heart : the most beautiful mother of all mothers "Fatima Al-Zahra", who has supported me in my life and gave me all the courage and help and plant in m ethe love work and gave me endless love no end.

To my dear father "Salim" who encouraged me and help me and gave the faith and the spirit of challenge and competition,

To my beloved and precious sister Israa

, to Sanadi in life Ahmad Iyad and Abdel Wahab,

to all my grandparents, may God have mercy on them.

To all my uncle, especially my uncle Nasser Ali Mohiuddin to My aunts and to every one in the family Lakehal and Amrani,

To My fiance Mohammed Al-Saleh, who gave me all the support in difficult times,

To My second sister and my beloved Fatima is the gift of God,

To all my friends.

RIHAB

THANKS

We thank God Almighty who gave us strength and care in completing this humble work

We also want to extend our sincere thanks to our dear Professor, our supervisor ***Dr. BELAKROUM Karima*** *for her patience, guidance, help and confidence, which has created in us a love of competition, diligence and perseverance and her generosityfor accepting the supervision of this work.*

We want to thank ***Dr. Noura BOUSSOUF*** *for her support and guidance, we also extend our thanks and appreciation to* ***Dr. BOURAS Nacer, and Dr. BATOUCHE Mouna*** *for the honor of attending the discussion.*

The achievements of this research by the research unit at the University of Frère Mentouri-Constantine 1, as well as the scientific research unit of the University of Kasdi Merbah-Ouargla.

We thank all who support usfrom near orfar, especially PhD students

G. Takrim , S. Mustafa and B. Safa

Abstract

The objective of this work is to prepare a high-temperature superconducting material for Phase Bi 2212 by solid reaction, and to study the effect of nickel doping in compound $Bi_2Sr_2CaCu_2O_{\delta+8}$ in different percentages 1%,3% and 5% , on the structural and optical properties, where the study based on the results given, showed with The UV-Vis spectra The energy gap is so small, from the order of 10^{-2} or 10^{-3}, that it can not appear in the spectrometer and show the sample to be conducting at room temperature with no band gap present at 300K, in X-ray diffraction it was found that , While in the SEM Nanometer grains combine to form clusters of micrometre dimensions, as the EDX results are Nickel is placed in sites tetrahedral or octahedral in the crystal lattice.

Key words: Bi 2212, high-temperature superconducting, solid reaction, nickel doping, X-ray diffraction.

الملخص

الهدف من هذا العمل هو إعداد مادة فائقة التوصيل ذات درجة حرارة عالية للطور Bi 2212 عن طريق التفاعل الصلب، ودراسة تأثير التطعيم بالنيكل في مركب $Bi_2Sr_2CaCu_2O_{\delta+8}$ بنسب مختلفة1 ٪ و 3 ٪ و 5 ٪ ، على الخصائص الهيكلية والبصرية ، حيث أظهرت الدراسة المستندة إلى النتائج المعطاة ، بمطيافية الأشعة UV-Vis أن فجوة الطاقة صغيرة جدا ، من ترتيب 10^{-2} أو 10^{-3}، حيث أنه لا يمكن أن تظهر في المطياف, وتظهر العينة أن تجري في درجة حرارة الغرفة مع عدم وجود فجوة الطاقة في 300K، في حيود الأشعة السينية وجد أن , بينما في المجهر الالكتروني الماسح الحبيبات النانومترية تتحد لتشكيل مجموعات من أبعاد ميكرومترية ، كما بينت نتائج EDX النيكل يتموضع في مواقع رباعي السطوح أو ثماني السطوح في شبكة البلورية.

الكلمات المفتاحية: Bi 2212, فائقة التوصيل ذات درجة حرارة عالية, التفاعل الصلب, التطعيم بالنيكل, حيود الأشعة السينية.

Résumé

L'objectif de ce travail est de préparer un matériau supraconducteur à haute température pour la phase Bi 2212 par réaction solide, et d'étudier l'effet du dopage au nickel dans le composé $Bi_2Sr_2CaCu_2O_{\delta+8}$ en différents pourcentages 1%,3% et 5% , sur les propriétés structurelles et optiques, où l'étude basée sur les résultats donnés, a montré avec les spectres UV-Vis que l'écart d'énergie est si faible, de l'ordre de 10^{-2} ou 10^{-3}, qu'il ne peut pas apparaître dans le spectromètre et montrer que l'échantillon est conducteur à température ambiante avec pas de bande interdite présente à 300K, en diffraction des rayons X, il a été constaté que, Alors que dans les grains nanométriques SEM se combinent pour former des amas de dimensions micrométriques, comme les résultats EDX sont Nickel est placé dans des sites tétraédriques ou octaédriques dans le réseau cristallin.

Mots clés: Bi 2212, supraconducteur à haute température, réaction solide, dopage au nickel, diffraction des rayons X.

INDEX

INDEX of figures

INDEX of tables

Introduction

General introduction

Superconductivity is the phenomenon of certain materials exhibiting zero electrical resistance and the expulsion of magnetic fields below a characteristic temperature. The history of superconductivity began with Dutch physicist Heike Kamerlingh Onnes's discovery of superconductivity in mercury in 1911. Since then, many other superconducting materials have been discovered and the theory of superconductivity has been developed. [7] These subjects remain active areas of study in the field of condensed matter physics. For more than 20 years and despite much research, the mechanism behind high temperature superconductivity in copper oxides, also called cuprates, remains an open problem. Due to the discovery of superconductivity in cuprates by Bernorz and Müller in 1986, considerable interest was shown in the characterization of their structural, magnetic and electrical properties. [8] While the critical temperature was 23 K in conventional superconductors, it now reaches 194 K under pressure in these new compounds.

The key structural element of cuprates, a category of superconducting materials with high critical temperature with a very large number of compounds, is nevertheless in simple appearance: planes made up of copper and oxygen atoms in which it is possible to add carriers. These CuO2 plans alternate with reservoir plans of charges. The properties of cuprates strongly depend on the electron density in these plans. The mixed valence state of copper, necessary for the appearance of superconductivity in cuprates, can be modified by adjusting the cationic substitutions or additions. Due to their low dimensionality and the strong electronic correlations between copper atoms, these compounds have original and very varied physical properties depending on the doping of the shots. In the absence of doping, they present an order low temperature antiferromagnetic. When doping increases, antiferromagnetism is destroyed and the planes become superconducting at low temperatures. At the same time, the normal state above their critical temperature and the superconducting state call into question respectively the theory of Fermi liquids and a usual BCS description, two models well suited to describe conventional metals and superconductors. [9]

Our study concerns the effects of addition on the structural properties, and optical of the compound $Bi_2Sr_2CaCu_2NixO_8$-δ (Bi2212). In the first chapter we take

a quick look at the physical phenomenon of superconductivity, its history and its main applications. The second chapter is a specific presentation of the Superconductors at High Critical Temperature (SHTC), to the crystal structure of bismuth-based cuprates and to the effect of additions in the Bi2212 phases. It also has a introduction to the characteristic properties of cuprates deduced from their diagram of temperature-doping phase, and also we describe the experimental characterization techniques used in the context of this thesis. The third chapter describes the procedure and heat treatments used for the preparation of the various samples of the Bi2212 phase, as well as the experimental results obtained are exposed and discussed. The structural study of the material is presented in detail in this chapter. The samples were structurally characterized by X-ray diffraction (XRD), scanning electron microscopy (SEM), X-ray Energy Dispersion (EDX) analysis.

Chapter 1: General informations about superconductivity

The superconductivity property is shown in some materials. The elements at a low temperature called critical heat with no electrical resistance and the expulsion of the applied magnetic field and this is what made them materials with applications not limited and we will try to understand and explain these phenomena.

1.Supraconductivity

SuperConductivity is the property that has certain materials to conduct the electric current without resistance provided their temperate is lower than a certain value called critical temperator (T_C) .we say that there is a transition from the normal state to the superconducting state .these supraconducting materials are also opposed to any external magnetic field

.

1.1.History of supracoductivity

For many years, it is known that the electrical resistance of a metal is proportional to its temperature. In 1911, the Dutch physicist Heike Kammerlingh Onnes in Leiden began cooling some mercury with liquid helium. He studied the resistance of metals at low temperatures and found that the resistance of mercury suddenly drops to zero when cooled below -269 ^{0}C (= 4 K) at 4.2 K.[10] The resistance of the metal completely disappeared and Onnes had discovered superconductivity. He was awarded the Nobel Prize in 1913 for liquification of Helium not specially for superconductivity. As the superconducting electrons travel through the conductor they pass unobstructed through the complex lattice. Because they bump into nothing and create no friction they can transmit electricity with no appreciable loss in the current and no loss of energy. Despite the broad range of compounds (both inorganic and organic) that are known to superconduct at very low temperatures, often below the boiling point of liquid helium, the highest superconducting transition temperature recorded before 1986 was 23.2 K for the alloy Nb3Ge. Below transition temperature $\mathbf{T_c}$,superconducting materials exhibit two characteristic properties:

- Zero electrical resistance (R = 0)
- Perfect diamagnetism (Meissner effect, χ= -1)

Remarkably, the magnetic behavior of a superconductor is distinct from perfect diamagnetism[1].

In 1957 Bardeen, Cooper, and Schrieffer (BCS) put forth a ground breaking microscopic description of superconductivity that incorporated all previous theories, and explained recent developments.[11] The essence of BCS theory is that electrons in a superconductor pair via a weak attractive interaction due tophonons (lattice vibrations) that exist naturally in the crystal lattice. Since electrons are fermions, when they pair they form bosons, which are not restricted by the Pauli Exclusion Principle, and can thus all condense into a single quantum state (same energy state) forming condensate named Bose-Einstein Condensation. these electron pairs, known as Cooper Pairs. BCS theory was the first quantum mechanical description of superconductivity [1]. A dramatic change and a great breakthrough occurred in 1986 when Bednorz and Muller discovered superconductivity around 35 K in the Ba-La-Cu-O system. Although this temperature was not very high, the discovery triggered the exploration of a whole class of similar materials, and transition temperatures above 90 K were soon reached in $YBa_2Cu_3O_{7-\delta}$. The discovery of Bednorz and Muller is break through because it crossed the BCS limit of transition temperature, T_c and called high temperature superconductors (HTSC)[1].

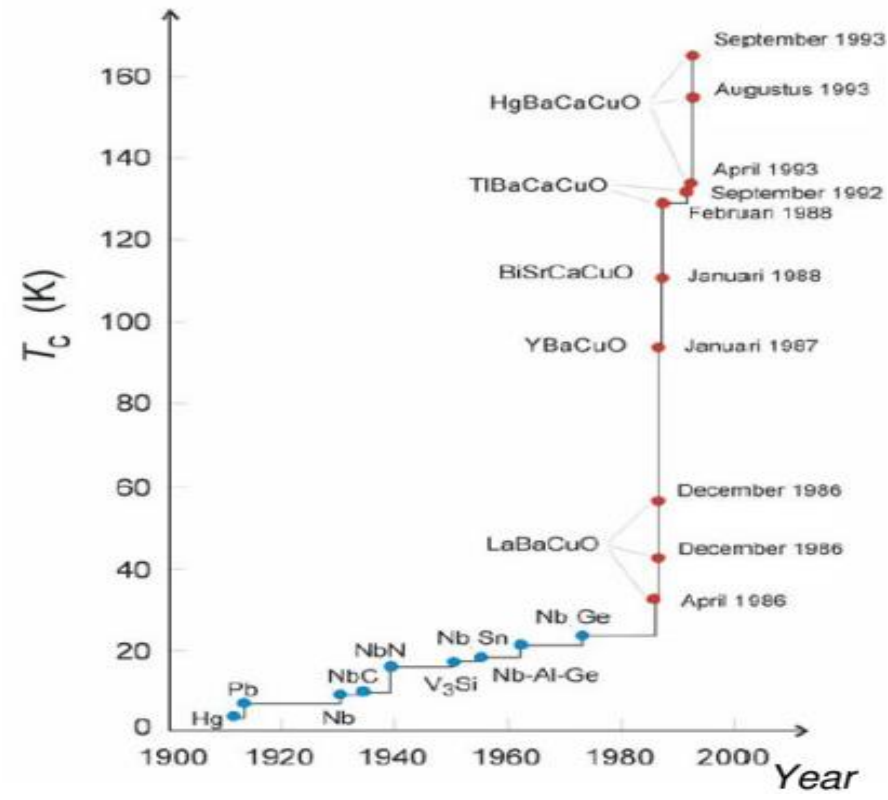

Figure1.1: Superconducting materials discovered in 20th century[2].

1.1.2.BCS theory

The concept of superconducting fluctuations will then be introduced. As mentioned above, the mechanism behind superconductivity was not understood until 1957, when Bardeen, Cooper and Schrieffer (BCS)[11] presented their detailed microscopic theory. Much earlier, however, many phenomena of superconductors could be well described using phenomenological models. The arguments in the BCS theory can be divided into three parts, which together explain superconductivity:

1. Electrons form pairs in the presence of an attractive force. If there is an attractiveinteraction between electrons at the Fermi surface, no matter how weak, stable pairs will form from electrons with mutually opposite wave vectors and opposite spins. The possibility of pair formation was pointed out already by Cooper [12], and the pairs are called Cooper pairs.

2. The attraction between electrons is caused by crystal-lattice vibrations (phonons). This part of the theory will probably have to be partly modified for the high-temperature superconductors.

3. An energy gap opens up in the electron density of states at the Fermi surface. In a simplified picture, resistive scattering of electrons in a superconducting material requires excitation across the energy gap, and cannot easily occur.

The original BCS theory only applies well to superconductors with weak electron-phonon coupling. Twenty years after the discovery of superconductivity in high-temperature copper oxide superconductors (HTSC), there is still no viable explanation as to what holds the electrons paired together in a Cooper pair. The main characteristics of HTSCs are very similar to the ones observed in classical superconductors, i.e. they show zero electrical resistivity and magnetic shielding (Meissner effect).

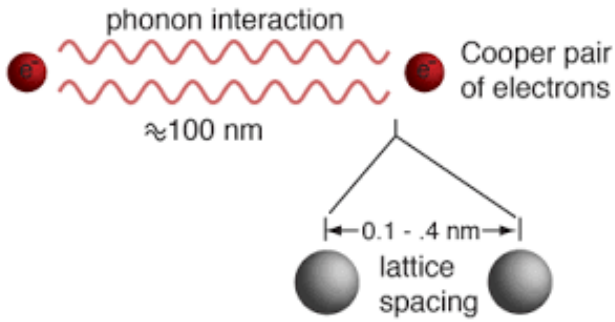

Figure1.2: Cooper pairs and BCS theory.

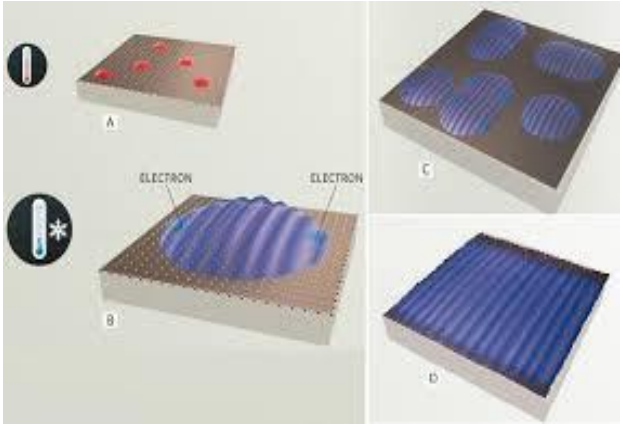

Figure1.3: Relation between temperateur and density of Cooper pairs.

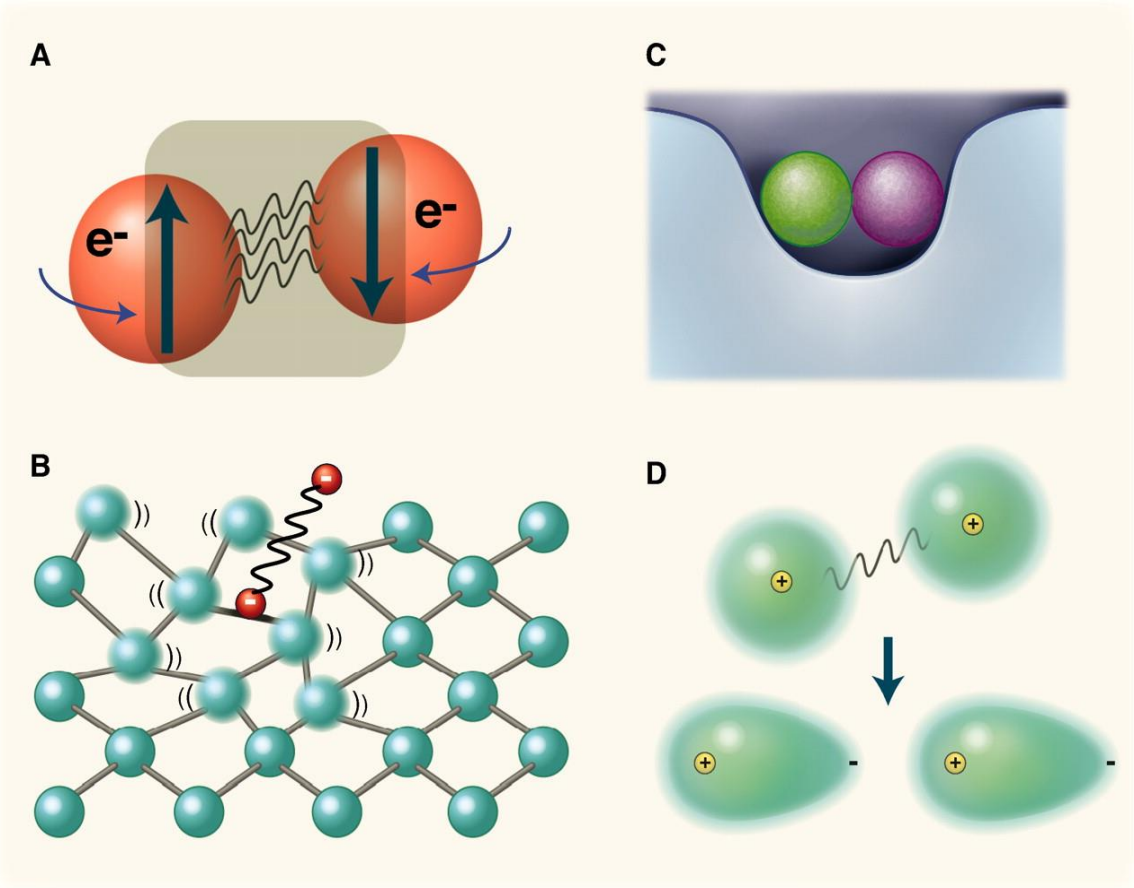

Figure 1.4: The Electron-Pairing Mechanism of Superconductors**.**

1.1.3.Paramagnetisme

It is the materials with unfilled layers in nature (families of Fe, Pd and Pt), it resulted in the non compensation of the orbital and spin moment so naissonce at a magnetic moment resulting for each atom in the overall magnetization of the material the moment tend to orient in the direction of the exciting field.

Since the orienting effect of the field is limited by thermal agitation, the resulting moment per unit volume is a function of temperature. however, there are some types of paramagnetism that are independent of temperature, especially one that is due to the spin of free electrons in metals (rare earths, iron group salt, Cr)

1.1.4. Meissner Effect

There is a magnetic link to superconductivity. It is called diamagnetism, another name for the Meissner Effect. The Meissner effect is the total exclusion of magnetic fields from the inside of a superconductor. It was discovered by Walter Meissner and Robert Ochsenfeld in 1933 [6]. They discovered that a superconducting material would repel a magnetic field. The Meissner effect shows that a magnet can be levitated over a superconductive material.

- Principe

We use a sample of superconducting materials to which we apply an external magnetic field of weak amplitude. At the same time cool the sample to a temperature lower than Tc . It is observed that when a superconductor is cooled in addition to the application of a weak magnetic field, the flow lines do not penetrate the material, so the internal magnetic field of the material is lacking. The Meissner effect is not characteristic of a methyl conductor characterized by zero resistance, Meissner and ochsenfeld interpreted this property of superconductors by the appearance of super-currents on the surface of the material creates a surface magnetic flux B that is exactly opposite to the external magnetic field :

$\vec{B} = 0 = \mu_0 \vec{H}_a + \vec{B}_s$ with $\vec{B}_s = \mu_0 \vec{M}$ and $\vec{M} = \chi \vec{H}_a$

From where $\mu_0 H_a (1 + \chi) = 0$ and $\chi = -1$ (1.1)

The superconducting material therefore exhibits perfect diamagnetism. This important result cannot be deduced solely from the fact that a superconductor is a zero resistivity.

According to ohm's law $\vec{E} = \rho\vec{j}$, it is noticed that if the resistivity ρ cancels, then $\vec{j}$ remains finite and $\vec{E}$ must tend to zero. Or according to Maxwell's equation, $\partial\vec{B}/\partial t$ is proportional to rot E, hence zero resistivity implies tha$\partial\vec{B}/\partial t = \vec{0}$. This wants everything simply say that the flux in the metal can only vary when cooled down to below the transition temperature. This is at odds with the Meissner effect and therefore suggests that a perfect diamagnetism is an intrinsic property of the superconducting state[4].

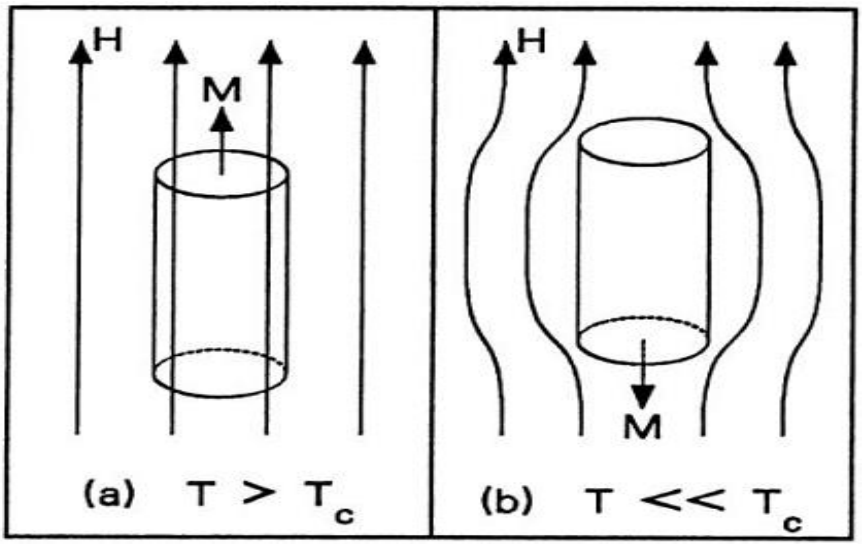

Figure 1.5: Effect of Meissner[5].

1.1.5.Zero resistivity

Superconductors have the ability to conduct electricity without energy loss. When the current enters an ordinary conductor, for example a copper wire, a certain energy is lost. In a light bulb or electric stove, the electrical resistance creates the light and heat.

1.1.6.Critical temperature

Is the temperature btween the normale state and the superconducting state.

1.2.Classifications of superconducting materials

Divided into two types:

1.2.1.Type I

For type I superconductors, there is only one critical magnetic field H_{C1}, and as well as two states: superconducting or normal. The magnetic field partially penetrates in the material on a length, called London length, in which develops super currents. Superconductors of this type are essentially pure bodies, such as mercury (Hg), indium (In), tin (Sn) and lead (Pb). In Figure 1 , the characteristic H(T) of a type I superconductor is presented. The critical field being relatively small since they do not exceed 0.2 Tesla, this explains that type I superconductors are of no interest practice in electrical engineering.The variation of the critical magnetic field H_C as a function of temperature T (Figure 1) (phase diagram) checks the following relationship:

$$H_C\,(T) = H_C^0\left(1-\left(\frac{T}{T_C}\right)^2\right) \qquad (1.2)$$

With H_C^0 the field at zero temperature

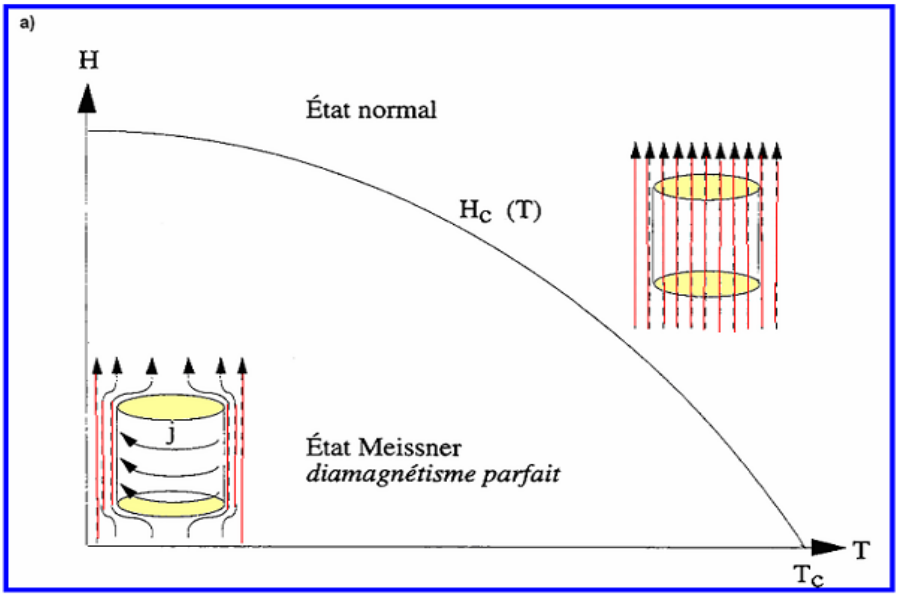

Figure 1.6: variation of the critical field as a function of temperature for a Type I superconductor.

1.2.2.Type II

These superconductors have two critical fields, Hc1 and Hc2 significantly higher than the first (up to several hundred Teslas in oxides). These present in addition to higher values of temperature, or critical field and current (Figure 1.). The presence of two critical fields makes things more complicated. Three zones to considered :

- **Zone 1** (**H** < $\mathbf{H_{c1}}$): The behavior is similar to that of type I superconductors.
- **Zone 2** ($\mathbf{H_{c1}}$ < **H** < $\mathbf{H_{c2}}$): The mixed state is characterized by partial penetration of the fieldmagnetic in the form of a vortex, and therefore partial diamagnetism.
- **Zone 3** (**H** > $\mathbf{H_{c2}}$): The material becomes normal again.

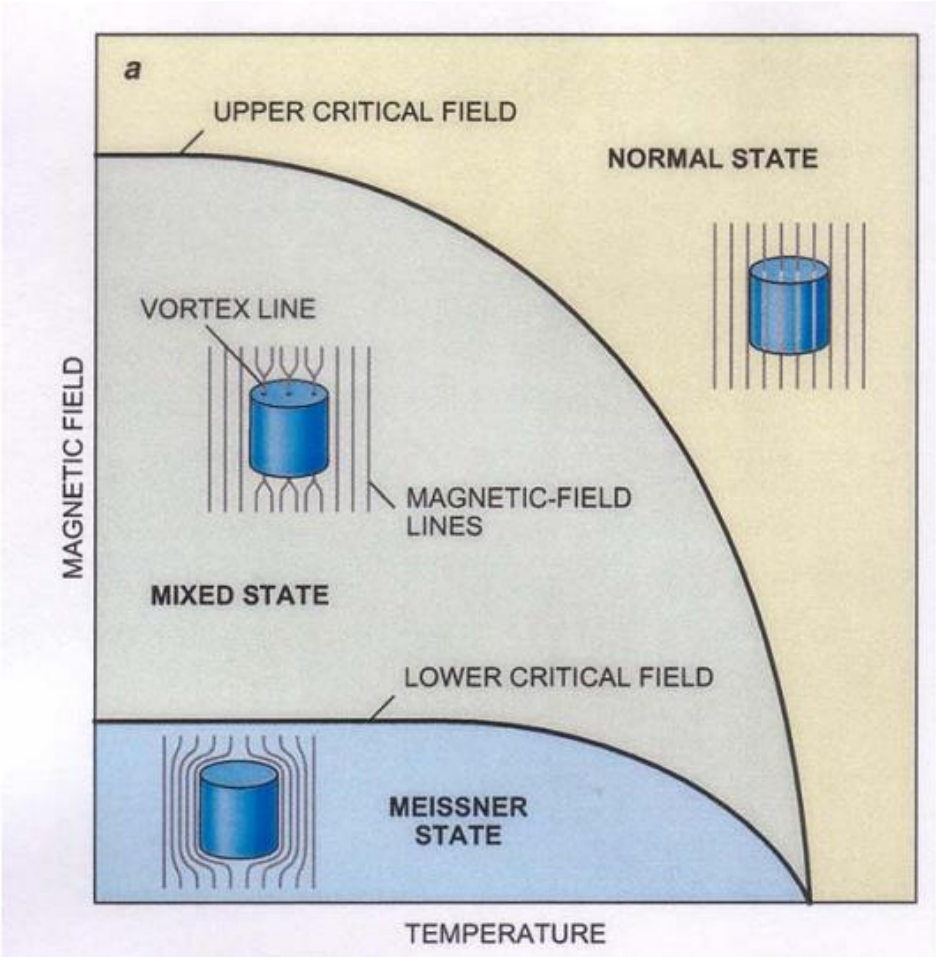

Figure 1.7: Variation of the critical field as a function of temperature for a Type II superconductors[5].

1.3.Materials supraconductivity

Materials supraconductivity appear in several different forms:

1.3.1.Simple elements

Superconductivity was first discovered in the simple elements mercury, then lead. After studying all the element of the periodic table, it was found that 54 element out of 101 element have the property of supercoductivity[3] at temperateures below the critical temperatur, as the latter differs from one another, some of these elemnts are in amorphous from and other in the from of films , on the other hand , the best metals (copper ,silver and gold) do not have this property.

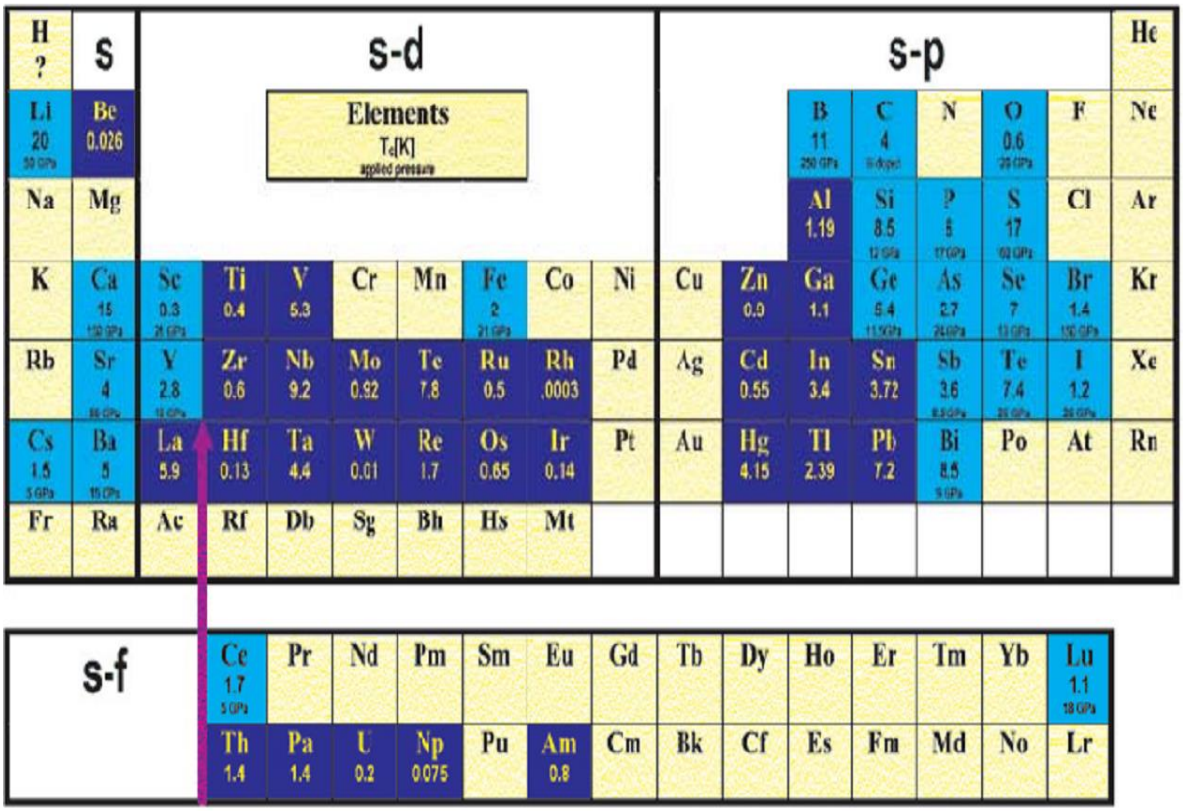

Figure1.8: Periodic table illustrating the distribution and critical temperature T_C of simple element for which superconductivity has been observed with or without the application of pressure (blue elements + sky blue elements = supercoducting elements)[3].

1.3.2.Alloys

The best representatives of this family of supercoductors are Niobium_Zirconium (Nb_Zr, T_C = 11 K) [3] and Niobium-Titanium (Nb_Ti, T_C = 9 K) [3] having a face centered cubic crystallographic structure, because these two materials remain, even today, the basic materials for most of the applications of superconductivity in the field of electrical engineering.

1.3.4.Carbides and Nitrides

These are compounds whose elements include carbon or nitrogen, as well as a hybrid compound that incloudes both carbon and nitrogen, where their total concentration is equal 1.

Table 1.1: characteristics carbide and nitride type superconductors.

Materiel	NbN	NbC	$Nb(C_{0.3}\ N_{0.7})$	HfN	MoC	MoN	ZrN	VN
T_C [K]	15.7	9.0	17.4	8.8	8.3	12	10	8.8

1.3.5.Organic superconductors

They are polymar chains made mainly of carbon and hydrogen containing metal element (see table 1.2).

Table 1.2: Characteristics of some organic superconductors.

Materiel	$(ET)_2Cu(NCS)_2$	$(ET)_2Cu[N(CN)_2]Br$	$(BEDT - TTF)I_3$
T_C [K]	10.0	11.2	8.1

1.3.6.Ceramics

Superconducting materials at high critical temperateures are given in Table1.3.

Table 1.3: Classification and reported Tc values of HTS compounds [3].

HTS Family	Stochiometry	Notation	Compounds	Highest T_c [K]
Bi-HTS	$Bi_mSr_2Ca_{n-1}Cu_nO_{2n+m+2}$ m = 1, 2 n = 1, 2, 3…	Bi-m2(n-1)n, BSCCO	Bi-1212 Bi-2201 Bi-2212 Bi-2223 Bi-2234	102 34 96 110 110
Pb-HTS	$Pb_mSr_2Ca_{n-1}Cu_nO_{2n+m+2}$	Pb-m2(n-1)n	Pb-1212 Pb-1223	70 122
Tl-HTS	$Tl_mBa_2Ca_{n-1}Cu_nO_{2n+m+2}$ m=1,2 n = 1, 2, 3 . . .	Tl-m2(n-1)n, TBCCO	Tl-1201 Tl-1212 Tl-1223 Tl-1234 Tl-2201 Tl-2212 Tl-2223 Tl-2234	50 82 133 127 90 110 128 119
Hg-HTS	$Hg_mBa_2Ca_{n-1}Cu_nO_{2n+m+2}$ m = 1, 2 n = 1, 2, 3 . . .	Hg-m2(n-1)n, HBCCO	Hg-1201 Hg-1212 Hg-1223 Hg-1234 Hg-1245 Hg-1256 Hg-2212 Hg-2223 Hg-2234	97 128 135 127 110 107 44 45 114
Au-HTS	$Au_mBa_2Ca_{n-1}Cu_nO_{2n+m+2}$	Au-m2(n-1)n	Au-1212	82
123-HTS	REBa2Cu3O7-δ RE = Y, La, Pr, Nd, Sm, Eu, Gd, Tb, Dy, Ho, Er, Tm, Yb, Lu	RE-123, RBCO	Y-123, YBCO Nd-123, NBCO Gd-123 Er-123 Yb-123	92 96 94 92 89
Cu-HTS	$Cu_mBa_2Ca_{n-1}Cu_nO_{2n+m+2}$ m=1,2 n = 1, 2, 3 . . .	Cu-m2(n-1)n	Cu-1223 Cu-1234 Cu-2223 Cu-2234 Cu-2245	60 117 67 113 < 110
Ru-HTS	$RuSr_2GdCu_2O_8$	Ru-1212	Ru-1212	72
B-HTS	$B_mSr_2Ca_{n-1}Cu_nO_{2n+m+2}$	B-m2(n-1)n	B-1223 B-1234 B-1245	75 110 85
214-HTS	E_2CuO_4	LSCO "0201" Electron-Doped HTS PCCO NCCO	$La_{2-x}Sr_xCuO_4$ Sr_2CuO_4 $La_{2-x}Ce_xCuO_4$ $Pr_{2-x}Ce_xCuO_4$ $Nd_{2-x}Ce_xCuO_4$ $Sm_{2-x}Ce_xCuO_4$ $Eu_{2-x}Ce_xCuO_4$	51 25(75) 28 24 24 22 23
	$Ba_2Ca_{n-1}Cu_nO_{2n+2}$	"02(n-1)n"	"0212" "0223"	90 120

			“0234“ “0245“	**105 90**
Infinite-Layer HTS	**$ECuO_2$**	**Electron-Doped I. L.**	**$Sr_{1-x}La_xCuO_2$**	**43**

1.4.Applications

Superconductors have got tremendous applications in various fields. Some of them are listed below:

Medical diagnosis -Magnets for MRI machines.

- ✓ Computing technology:
- ✓ Cryotrons.
- ✓ Memory devices.
- ✓ Electronics and measuring technology:
  - Bolometer-receivers of thermal radiation.
  - Superconducting magnetic lenses.
  - c) Masers.
- ✓ Nuclear power and space
  - Magnets for thermonuclear reactions
  - Elementary particle accelerators.
  - Bubble chamber
  - Resonance pumps
  - Gyroscopes.
  - Magneto hydrodynamic (MHD) generators.
  - Protection of astronauts from radiation.
  - Superconducting Magnets for particle AcceleratorBackground and Motivation
- ✓ Transport and communication:
  - Levitating trains.
  - Magnetic levitators.

References

[1]. Mohanta, A., Superconducting order parameter fluctuation in doped and composite cuprate superconductors, 2011.

[2]. Gilioli, E. and F. Pattini, Growth of oxide thin films for energy devices by Pulsed Electron Deposition.

[3]. Hott, R., et al., Superconducting materials—A topical over*view*. Frontiers in Superconducting Materials, 2005: p. 1-69.

[4]. Mahtali, M., Etude et caractérisation de structures supraconductrices. 2007.

[5]. Weh, Z., Magnetic Properties of High Temperature Superconductors. NSF Grant DMR

[6]. W. Meissner, R. Ochsenfeld, Naturwissenschaften 21, 787 (1933).

[7]. H. Kamerlingh Onnes, Leiden Comm. **120b, 122b, 124c** (1911).

[8]. G. Bednorz and K. A. Müller, Z. Phys. **B64**, 189 (1986).

[9]. BOUSSOUF,N., Effet du dopage dans les céramiques supraconductrices de Bi2Sr2CaCu2O8+δ,2011.

[10]. H.K. Onnes, Communications from the Physical Laboratory of the University of Leiden (1911).

[11]. J. Bardeen, L.N. Cooper, and J.R. Schrieffer, Physical Review, 108 (1957) 1175.

[12]. L. N. Cooper, Phys. Rev. 104 (1956) 1189.

Chapter2: Effect of doping on crystallographic structure and methodes of caharacterization

In this chapter, we present the effect of doping on crystallographic structure and the different methods of cauterization used to analyses our samples.

2. High Critical Temperature Superconductors (HCTS)

The HCTS are almost all cuprates, that is, compounds based on copper oxide CuO. They generally have one or more CuO2 planes in their structure. The various theoretical models attribute to them particular properties. Thus, YBaCuO and bismuth compounds are ceramics possessing a fairly complex mesh and a strong anisotropy due to the superposition of the superconducting CuO2 planes (called ab planes) and insulating planes. These insulating planes have two functions: to stabilize the crystallographic structure of the whole and to constitute a reservoir of charges for the superconducting planes.

2.1. General properties

2.1.2 Structure

The structure of all cuprates has one or more cubic perovskite-like blocks: a copper atom at the center of a CuO6 octahedron, at the vertices of which are oxygen atoms. This octahedron is itself centered in a cubic mesh. The CuO2 plane is the plane that contains the copper atoms of the perovskite block. Octahedra form a generally square network sharing their vertices and have quadratic symmetry The materials can thus be classified according to the number of CuO2 layers and we have for example:

-Single layer materials: Bi2Sr2CuO6+d (Bi2201), HgBa2CuO4+d (Hg1201), and La2-xSrxCuO4 (LSCO)];

-Tri-layer materials: Bi2Sr2Ca2Cu3O10+d (Bi2223) and HgBa2Ca2Cu3O8 + d (Hg1223) [29].

The number of CuO2 planes has a direct correlation with the superconducting properties. In general, the critical temperature Tc increases when the number n of CuO2 layers increases. This rule is verified in the same family of compounds such as those containing bismuth for example. Many cuprates, such as Y123 and Bi2212, have a slight orthorhombic distortion. Cuprates are classified according to the main element (Y, Bi, La, Tl, Hg, etc.) involved in the formula.

2.1.3. Anisotropy

Due to the structure of SHTC compounds, electrons move easily in some directions, and with difficulty in others. This property is the consequence of structural anisotropy which results in the anisotropic behavior of the critical current density and the critical magnetic field [9]. The critical current density is high when the direction of the current is along the CuO2 planes but two to three orders of magnitude smaller when this direction is perpendicular to these same CuO2 planes. This is due to the fact that the passage of the super current through the insulating layer of metal oxide is carried out by tunnel effect. Likewise, the critical magnetic field is much higher when it is applied in the direction perpendicular to the planes than in that parallel to these same planes [10,11].

2.1.4. Crystal structure of bismuth-based cuprates

The family of compounds Bi2Sr2Can-1CunO2n + 4 (or BSCCO system) consists essentially of three superconducting phases: Bi2201, Bi2212 and Bi2223 [12]. Parmi ces phases, la première phase découverte est la phase (Bi2212) en 1988 [13]. In the structure of compounds of this family, containing n CuO2 planes per half-cell:

-The CuO2 planes are responsible for the superconducting properties;

- The two BiO plans play the role of charge reservoir;

- Additional SrO plans ensure the stability of the structure

From n = 2, the planes of the Ca atoms are inserted between the neighboring planes of CuO2

The structure of these compounds is often orthorhombic with very close a and b lattice parameters (which sometimes qualifies the structure as pseudo tetragonal), while the parameter c varies according to the phase. The lattice parameter c varies, to a greater extent, as a function of the oxygen content as well as of the cationic composition. The role of copper and oxygen atoms depends on their position in the elementary cell

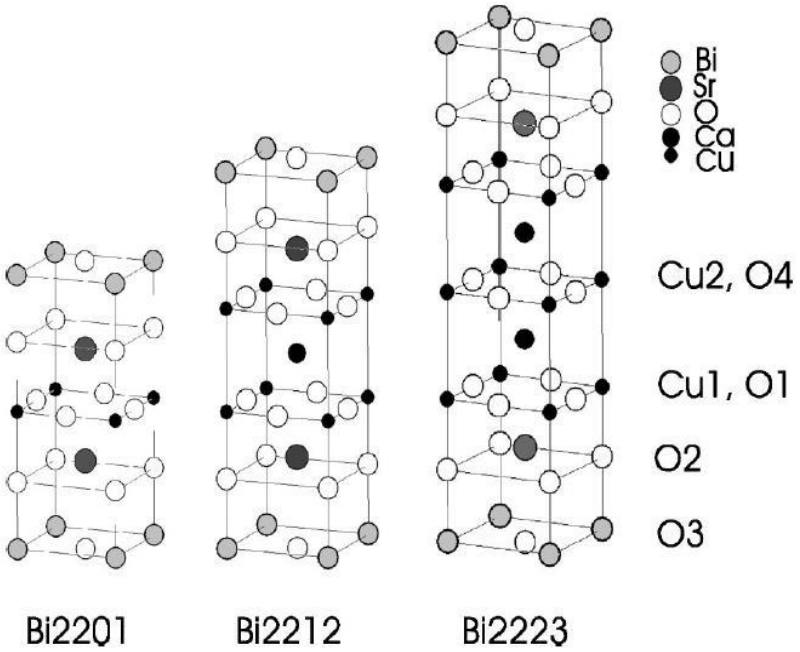

Figure 2.1: Notations used for copper and oxygen atoms in the cell unit of the three phases of bismuth-based cuprates [14].

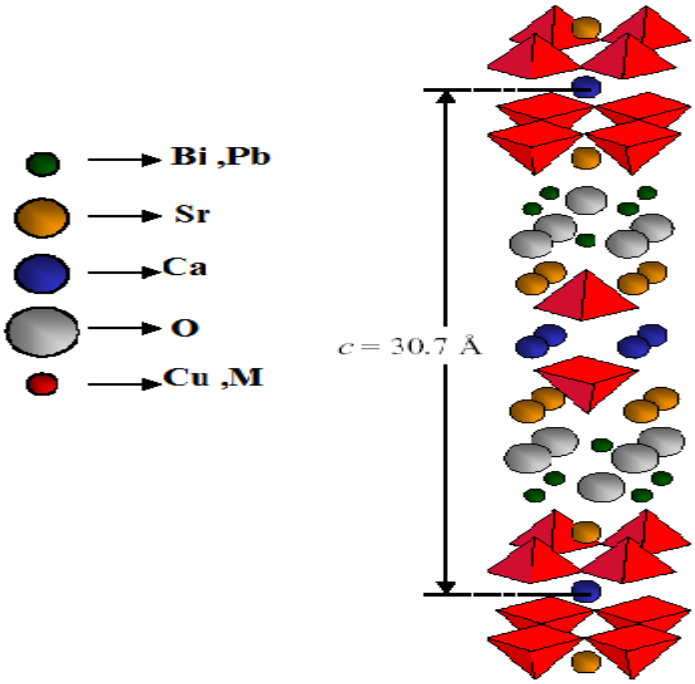

Figure. 2.2. Crystallographic structure of the Bi2212 phase [15]

2.2. Electronic properties of superconducting cuprates

Most of the electronic properties take place in the CuO2 planes. These plans, separated by load reservoir planes, differ from one system to another.

2.2.1. The CuO2 plans

The CuO2 plane is considered by the majority of authors to be responsible for superconductivity at high critical temperature. The CuO2 plane is composed of pyramids [16], formed by oxygen atoms, where the cation of the copper atom is in the center of the basic plane. The copper atoms in the CuO2 planes are much closer to the oxygen atoms in the plane (1.9 Å) than to the oxygen atoms in their vertical (2.4 Å). The overlap between orbitals of copper atoms and oxygen atoms is important. It allows doping of the CuO2 planes by variable number of holes, via a charge transfer mechanism between the oxygen atoms and the charge reservoir planes (Fig. II.5). The number of holes, transferred from the charge reservoir planes to the CuO2 planes [17,18], controls the electrical properties of these materials

2.2.2. Doping and phase diagram

Depending on the number of charge carriers in the CuO2 planes, all high critical temperature superconductors (SHTC) based on copper oxide have a phase diagram (T, doping). The electronic properties vary from an antiferromagnetic region to a Fermi liquid passing through the superconducting region. This phase diagram shows several areas. In the absence of doping or for very low doping, and below a TN temperature, the compound is a Mott insulator with an antiferromagnetic order The gradual increase in the holes in the CuO2 planes, causes a transition from the antiferromagnetic insulating compound to a metallic compound where the antiferromagnetic order is lost. From a certain doping value, the compound becomes superconducting. Le domaine de dopage où le composé est supraconducteur peut se diviser en deux parties : sous-dopée et sur-dopée. The critical temperature increases with doping to a maximum in the under-doped region, peaking in the region, corresponding to a so-called "optimal doping to then decrease to zero in the over-doped region.

In the under-doped region and above the TC line (in the area where the compound is in its normal state), a new line, corresponding to the suppression (or freezing) of low energy electronic excitations, may be traced.

The temperature corresponding to this line is denoted T *. This passage is known as the "opening of a pseudogap" [19]

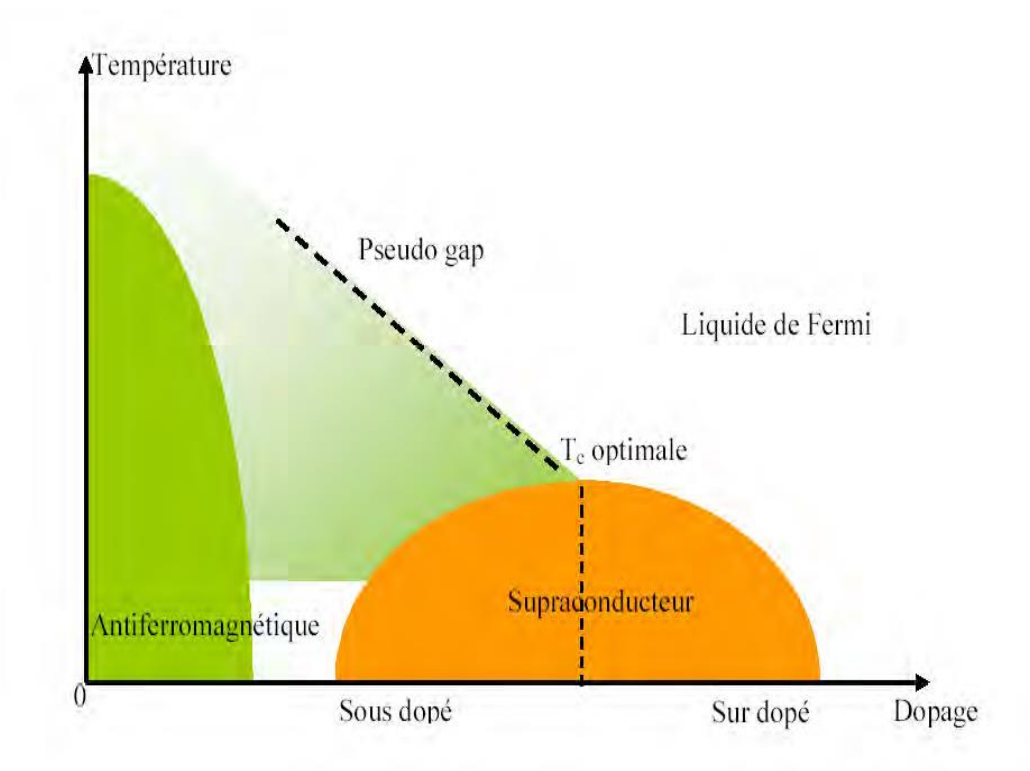

Figure2.3: Phase diagram of cuprates [20].

2.2.3.Antiferromagnetic region

The magnetic properties [21] of cuprates derive from the d electrons of the copper cations of the CuO2 planes and from the way in which the copper and oxygen atoms are ordered in the perovskite structure. Some specific properties of CuO2 plans explain the originality of SHTC:

-3d9 electronic configuration of Cu2 + transition ions and their positioning in an oxygen octahedron; these ions have a single hole on an x2-y2 type d orbital; the low value ½ of the spin of Cu2 + reinforces the effects of quantum fluctuations of the spin;

-A very strong covalency between Cu2 + ions and O2- ions, linked to the geometry of the planes (the Cu and O ions are aligned and separated by 1.9Å) and to the fact that the electronic levels of oxygen and copper are the most relatives; this covalency corresponds to the hybridization between the dx2-y2 orbital of copper and the 2pσ orbital of neighboring oxygen which points in the Cu-O-Cu axis

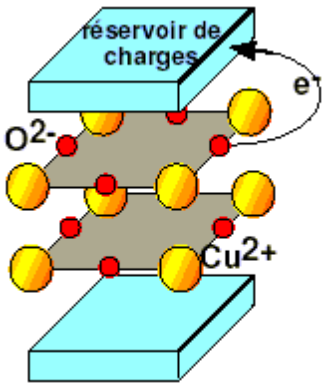

Figure. 2.4. Schematic representations of CuO2 planes [22,23]:
Charge transfer between the O2- ions (shown in red) and the charge reservoirs;

2.3. Effect of doping in cuprates

Doping is the most effective operation to modify the properties of Superconductors. There are two ways to dope the compound: either by substituting one cation by another of different valence as in La2-xSrxCuO4, where we substitute La3 + by Sr2 + and in Y1-yCayBa2CuO7-δ [24,25], or by adding additional oxygen as in Bi2212 where, after different annealing under oxygen, oxygen is inserted into the planes BiO. The last method is also used in HgBa2CuO4 + δ, TlBa2CuO6 + δ and La2CuO4 + δ. In all cases, doping corresponds to a transfer of charges from the reservoir blocks.towards CuO2 plans [26]. This mechanism is illustrated in figure 2.5. Doping can be measured by three methods:

- The thermoelectric power at 300K, which decreases linearly as a function of p, except in the case of LSCO [27];
- The Hall effect at low temperature, or more particularly the renormalized Hall effect RHeN / V where eN / V is the volume charge density per copper atom [28];

- The critical temperature Tc, knowing the critical temperature at optimal doping,with the relation :

$$\frac{TC}{Tmax} = 1 - 82.6(p - 0.16)^2$$

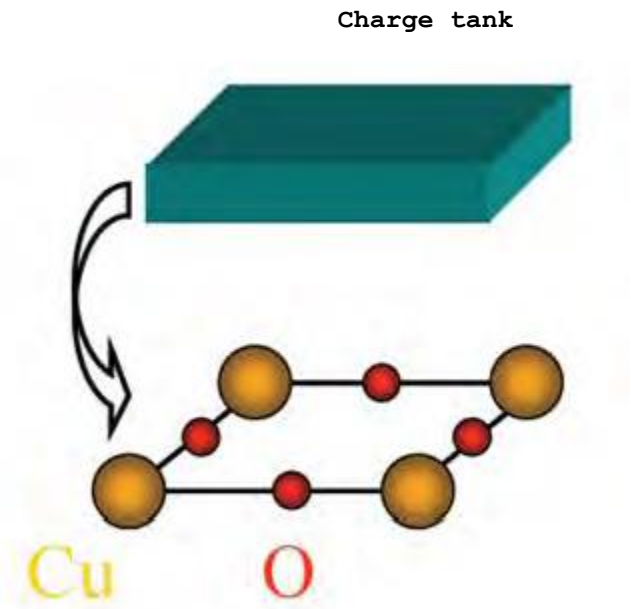

Fig.2.5: Schematic representation of the CuO2 planes surrounded by the Charges tank making it possible to vary the number of charge carriers within the cuprates.

2.4.Effects of doping

Doping can:

- Bringing a positive hole or an electron to the oxide superconductor;
- Improve the formation of the desired phase;
- Create vortex trapping centers ;
- Addition of MgO to the Bi2223 phase can reduce grain size by limiting the dissemination of the various elements [29].

Doping with manganese results in a lowering of the partial fusion temperature

Trapping of electrons is also improved.

The addition of silver in the powder of the Bi2223 phase improves the morphology by Elimination. Ag does not destroy superconductivity, and could even improve it. In addition, it

seems that this element improves the superconductivity following its diffusion between the grains. Iron rapidly destroys superconductivity by substitution at sites crystallographic Cu. The mixed valence state of copper, necessary for the appearance of superconductivity in cuprates, can be obtained by playing on cationic substitutions or on the modification of the anion network. The last method consists of replacing oxygen with other monovalent elements such as halogens for example or to insert these spaces. It has been established that the introduction of Zn into CuO2 planes can generate moments magnetic areas and Zn impurities can therefore no longer be considered as non-magnetic impurities.

2.5. Characterization techniques

To determine the structure, the different phases formed and the morphological variation microstructures during heat treatments, we used the techniques of following characterizations:

- X-ray diffraction (XRD) and mesh determination using software DicVol 04;
- Scanning electron microscopy (SEM) and EDX
- For optical caracterization we used the Ultraviolet–visible spectroscopy

2.5.1.X-ray diffraction (XRD)

X-ray powder diffraction (XRD) is a rapid analytical technique primarily used for phase identification of a crystalline material and can provide information on unit cell dimensions. The analyzed material is finely ground, homogenized, and average bulk composition is determined.

2.5.2.Fundamental Principles of X-ray Powder Diffraction (XRD)

Max von Laue, in 1912, discovered that crystalline substances act as three-dimensional diffraction gratings for X-ray wavelengths similar to the spacing of planes in a crystal lattice. X-ray diffraction is now a common technique for the study of crystal structures and atomic spacing. X-ray diffraction is based on constructive interference of monochromatic X-rays and a crystalline sample. These X-rays are generated by a cathode ray tube, filtered to produce monochromatic radiation, collimated to concentrate, and directed toward the sample. The interaction of the incident rays with the sample produces constructive interference (and a

diffracted ray) when conditions satisfy Bragg's Law ($n\lambda=2d \sin \theta$). This law relates the wavelength of electromagnetic radiation to the diffraction angle and the lattice spacing in a crystalline sample. These diffracted X-rays are then detected, processed and counted. By scanning the sample through a range of 2θangles, all possible diffraction directions of the lattice should be attained due to the random orientation of the powdered material. Conversion of the diffraction peaks to d-spacings allows identification of the mineral because each mineral has a set of unique d-spacings. Typically, this is achieved by comparison of d-spacings with standard reference patterns. X-rays have been discovered by Wilhelm Conrad Röntgen in Würzburg, Germany. On November 8, 1895, he conducted experiments including Crookes tubes, which are typically used to visualize streams of electrons[2]. X-rays belong to the group of electromagnetic rays, hence, they follow the rules of electromagnetic radiation. Electromagnetic radiation transports energy, also called radiant energy[2]. It can either be represented by photons or by a wave model. The wavelength can also be represented by frequency fp and the waves propagation speed, i. e., the speed of light c_0.

X-ray diffraction is a multi-function technique used to identify the crystalline phases of material and to analyze structural properties.

- .X-rays are produced in an X-ray tube.
  - The energy distribution of the photons is modified by inherent and additional filtration.
- The X-rays are attenuated differently by the various body tissues.
  - Scattered radiation, which impairs image contrast, is reduced.
- The transmitted photons are detected.
  - The image is processed and – in the case of CT – reconstructed.

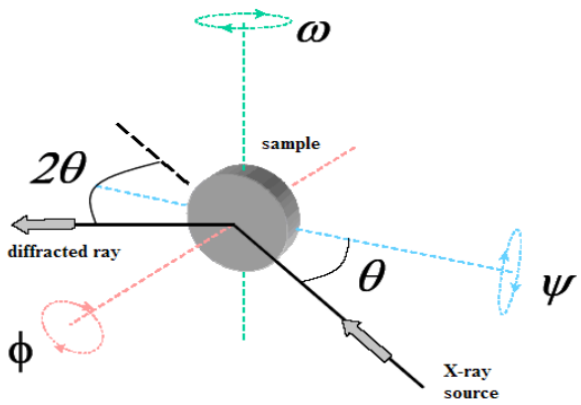

Figure 2.6: Geometry of X-ray diffractometry[3].

In our work, and in order to characterize our samples, we used a Bruker D8 Advanced type diffractometer using X-rays coming from the K α emission of Copper with a length of λ = 1.5402 Å as is shown in figure2.7.

Figure2.7:.Bruker D8 Advanced type diffractometer [Laboratory of Crystallography, University of the Mentour-Constantine brothers]

2.5.3. Program MAUD

This international school will cover many aspects of the “Combined Analysis” by X-ray, neutron and electron scattering and X-ray fluorescence applied to material science, ranging from fundamental requirements to technically relevant industrial and academic applications.

The combined analysis method has been developed over the years starting from the Rietveld method, extending it to most of the powder diffraction analyses and more recently incorporating, on the same idea, other techniques such as reflectivity, X-ray fluorescence and electron diffraction.

- **Description**

❖ Multipurpose Rietveld analysis program for Material Science including[30]:

– Crystallography.

– Quantitative analysis.

– Texture, Residual Stresses.

– Reflectivity, Layered systems.

– Microstructure.

❖ Easy to use interface including[30]:

– Wizard for automatic analyses.

❖ Connection to databases and use of the CIF syntax[30].

❖ Ability to suggest measurements and to drive them locally or remotely[30].

❖ Possibility to run[30]:

– Embedded in a browser over the internet.

– Locally as an application.

– On every platform.

❖ Plug-in structure to extend easily some features[30].

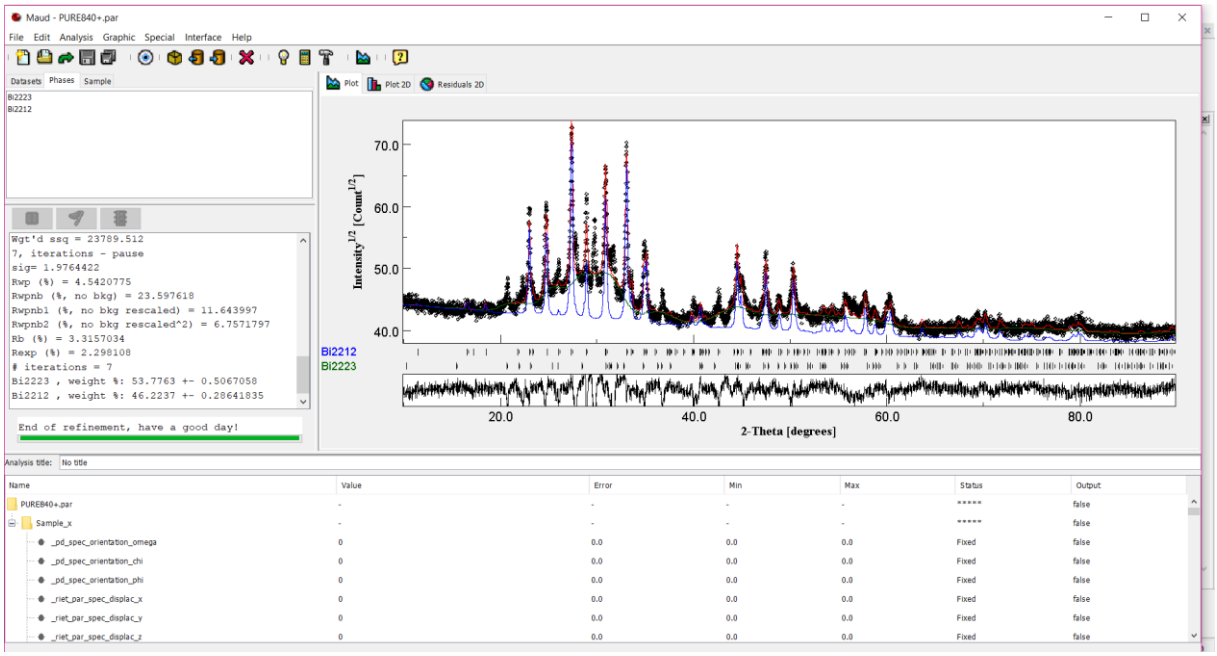

Figure2.8: MAUD window(refinement steps).

2.5.4. Scanning electron microscopy (SEM)

Scanning Electron Microscope images give information around the tomography, morphology, composition and crystallographic information of the specimen. The surface features of an object or "how it looks", The shape, size and arrangement of the particles making up the object that are lying on the surface of the sample or have been exposed by grinding or chemical etching; The elements and compounds the sample is composed of and their relative ratios, The arrangement of atoms in the specimen and their degree of order; just useful on single-crystal particles. Through the electron beam-sample interactions, secondary products like secondary electrons, backscattered electrons, X-rays, heat and light will be formed. Detectors collect backscattered electrons and secondary electrons and convert them into a signal that is sent to a screen where the image is formed[3].

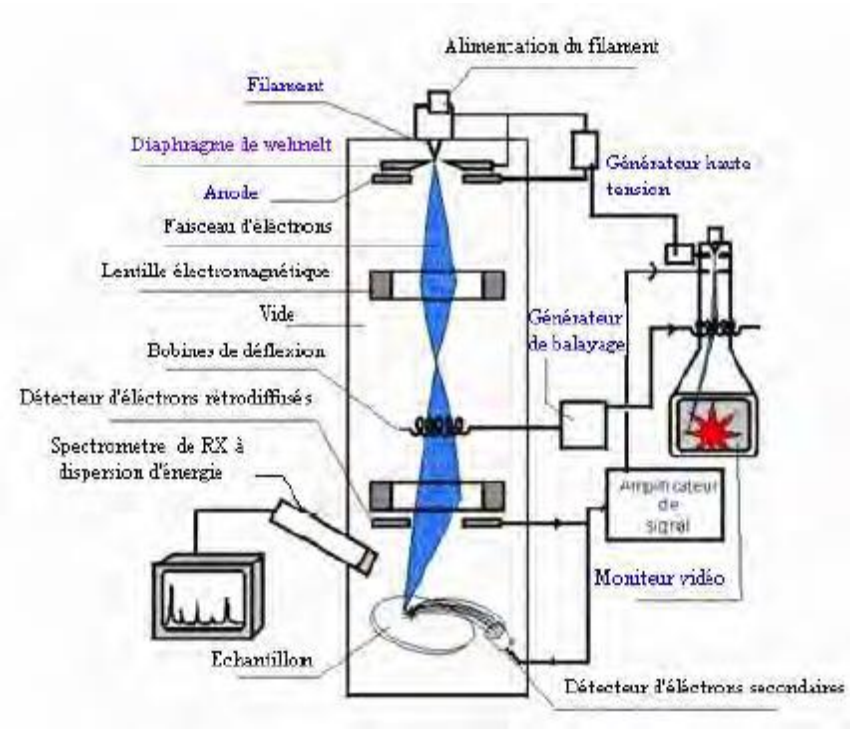

Figure2.9: Operating principle of a scanning electron microscope

The MEB used of the JEOL brand type JSM-6390-LV equipped with a electron beam lithography (Raith ELPHY Quantum) is at the CRAPC-Ouargla. It allows to visualize the granular state and, when it is the case, the crystallinity of samples. The analysis that is done is a surface analysis. Analysis of deeper layers can only be done after modification of the sample by a chemical attack or cut. We have used enlargements of 1000 and 5000 which clearly reveal the texture characteristics of each observed polycrystalline sample The observations were made at room temperature. The electron beam follows a vertical path through the microscope, in vacuum. The beam travels through electromagnetic fields and lenses, which focus the beam down-ward the sample. Once the beam hits the sample electrons will scatter through the specimen within a defined area called the interaction volume. These interactions can be divided into two major categories: elastic interactions and inelastic interactions.

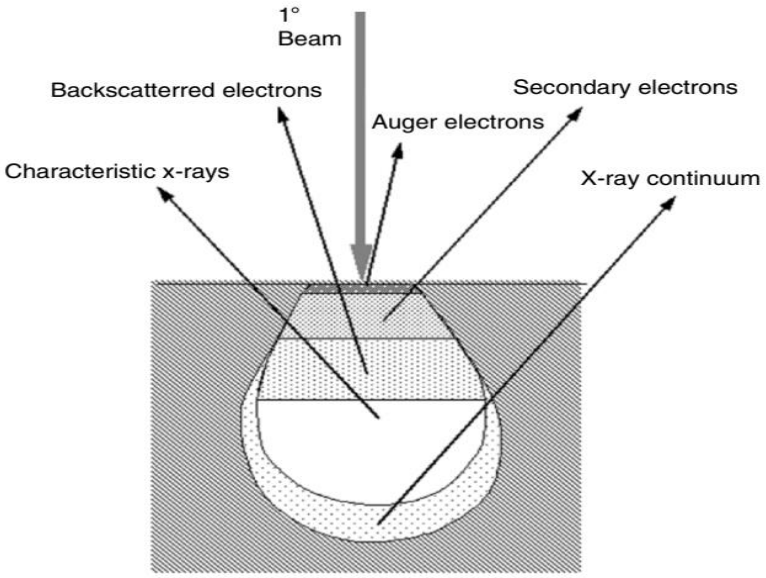

Figure 2.10: Interaction between the e-beam and the sample surface[8].

Particles emittedthe 3 types of particles emitted:

- **The electron sconder:** Are electrons torn frome the inner layers of the atoms of the electron by by the interaction of radiation applied , plus the electrons incidents which change direction and are energy.
- **Electrons backscattered:** are incident electrons that change direction with no energy change after interaction.
- **Auger electrons :** its of the electrons arrowed to the outer couch of the sample atoms by absorbed the fluorescence X-rays of the same atom.

Figure.2.11: Photo by MEB from CRAPC-Ouargla

2.5.5. Electronic microanalysis (X microprobe)

X-ray microanalysis allows elementary analysis by detecting the characteristic X lines of the elements present. It allows one-off analyzes with a spatial resolution of the order of 1 μm3. There are two techniques of X microanalysis:

- wavelength dispersion spectrometry (or WDS: Wavelength Dispersive Spectrometry)
- The identification of the elements constituting the target sample, from their X emission spectrum, was suggested in 1913 by Henry Moseley who found that the frequency of the characteristic lines emitted was a function of the atomic number of the emitting element.

2.5.6.Ultraviolet–visible spectroscopy

Ultraviolet radiation below 200Nm is called vacuum because air absorbs it so strongly and was discovered by physicist Victor Schumann in 1893[4]. UV–Vis spectroscopy occurs in a narrow range of the electromagnetic spectrum, and consists of visible and ultraviolet light. The visible spectroscopy consists mainly of the molecules or matter that absorb visible light wavelengths and frequencies[5]. The specific peaks can be seen by comparing with the standard of the matter and give sufficient information on the characterization of a matter in a mixed solution. UV spectroscopy is based on the UV radiation absorption of a sample, occurring from the electron transition from lower electronic states to higher electronic[5]. there are four types of transitions: 1.$\sigma \rightarrow \sigma^*$ transition; 2.n$\rightarrow \sigma^*$ transition; 3. n$\rightarrow \pi^*$ transition; 4.$\pi \rightarrow \pi^*$ transition[5].In our work, we used a spectrophotometer (UV3101PC type Shimadzu) recording double beam (UV-Visible), it is made up of three main parts: the source of the radiation, the sample holder, and the measuring system, on figure 2.8 is given the image of the spectrometer used.

Figure2.12: Dispositif expérimental de la spectroscopie UV-visible [CRAPC-Ouargla]

References

[1]. NAVARRETE, L.R.O., INSTITUT POLYTECHNIQUE DE GRENOBLE, 2009.

[2]. Berger, M., Q. Yang, and A. Maier, X-ray Imaging. Medical Imaging Systems, 2018: p. 119-145.

[3]. Gilioli, E. and F. Pattini, Growth of oxide thin films for energy devices by Pulsed Electron Deposition.

[4]. Ozaki, Y. and S. Kawata, Far-and Deep-ultraviolet spectroscopy2015: Springer.

[5]. Koç, M. and E. Karabudak, History of spectroscopy and modern micromachined disposable Si ATR-IR spectroscopy. Applied Spectroscopy Reviews, 2018. ***53****(5): p. 420-438.*

[6]. Hasegawa, T., Quantitative infrared spectroscopy for understanding of a condensed matter2017: Springer.

[7]. Shipp, D.W., F. Sinjab, and I. Notingher, Raman spectroscopy: techniques and applications in the life sciences. Advances in Optics and Photonics, 2017. ***9****(2): p. 315-428.*

[8]. Zhou, W., et al., Fundamentals of scanning electron microscopy (SEM), in Scanning microscopy for nanotechnology2006, Springer. p. 1-40.

[9]. T. P. Sheahen, « Introduction To High-Temperature Superconductivity» pp. 149-150, Eds. Kluwer Academic Pub.(1994).

[10]. Daniel Schneider, «These de doctorat», Swiss Federal Institute of Technology, Zürich, (2000).

[11]. Thomas Frello, « Structural and Superconducting Properties of High-Tc Superconductors », Risø National Laboratory, Roskilde, Risø–R–1086 (EN), Denmark January (2000).

[12]. S. Chu, Michael E. McHenry, J. Mater. Res 13, 589-595 (1998).

[13]. T. J. Lee, C. F. Huang, C. C. Teo, T. S Khor, H. C. Ku, K. W. Yeh, Y. Huang, H. H. Hung, Kiwako Sakabe, and Noriyoshi Sakabe, Chinese Journal of Physics 38,243-261 (2000).

[14]. N.N.Kovaleva, A.V.Boris, T.Holden, C.Ulrich, B.Liang, C.T.Lin, B.Keimer, et C.Bernhard, Physical. Rev B, 69, 054511 (2004).

[15]. Andrés Felipe Santander-Syro, « Structure électronique des cuprates supraconducteurs surdopés: étude par spectroscopie infrarouge et par ARPES », Laboratoire de Physique des Solides UMR 8502, Orsay.

[16]. Bruno Pignon, « Thèse pour obtenir le grade de docteur de l'université de tours », Université de Tours, (2005).

[17]. Philippe Bourges, « Thèse de doctorat », Université de Paris Sud Centre d'Orsay, (2003).

[18]. Julien Bobroff, « Thèse de doctorat », Université de Paris-Sud, U.F.R. Scientifique

[19]. J. Robert Schrieffer et James S. Brooks, « Handbook of High-Temperature Superconductivity Theory and Experiment », pp. 347-348, Springer, (2007).d'Orsay, (1997).

[20] . W. Guyard, « Rapport de pré thèse », Université Denis Diderot, Paris VII, (2005).

[21]. Julien Bobroff, « Recherches, Spécialité Sciences Physiques », Université Paris Centre d'Orsay Habilitation, (2004).

[22]. Philippe Bourges, « Thèse de doctorat », Université de Paris Sud Centre d'Orsay, (2003).

[23]. Thomas A. Maier, «The role of Zinc impurities in high-temperature superconductors», Poster, University of Cincinnati, (2002).

[24]. D.T.Verebelyi, C.W.Schneider, Y.K.Kuo, M.J.Skove, G.X.Tessema, J.E.Payne, Physica C328, 53-59 (1999).

[25]. Y.K.Kuo, C.W.Schneider, M.J.Skove, M.V.Nevitt et G.X.Tessema, Phy.Rev.B 56, 6201-6205 (1997).

[26]. http//: x x x.lanl.gov/pdf/ cond-mat/9902355 (1999).

[27]. S. Chakravarty « High Temperature Superconductivity», Addison-Wesley, Reading, MA, p. 136 (1990).

[28]. M.W.Hooker et L.Martin, «Preparation and Properties of High-Tc, Bi-Pb-Sr-Ca-Cu-O Thick Film Superconductors on YSZ Substrates » NASA Contractor Report 4761, Engineering & Sciences Company, Hampton, Virginia, (1996).

[29]. M.K.Yu, J.P.Franck, Phys.Rev.B 48, 939- 944 (1993).

[30]. Luca Lutterotti, Maud: A Rietveld Analysis Program Designed for the Internet and Experiment Integration, Acta Crystallographica Section A Foundations of Crystallography, August 2000.

Chapter3: Results and discussion

Depending on the desired application (electrical, magnetic), there are a large number methods for producing polycrystalline functional oxides, either in the form of powders, either of compacted ceramics, or of thin or thick layers. We used the solid state or solid state reaction method for the synthesis of our samples. This method consists in mixing powders of oxides or carbonates of the constituent cations of the ceramic and in reacting them by heat treatment, possibly in several stages, with intermediate grinding It has the advantage of simplicity and allows, with a few basic precautions, good control of cation stoichiometry. It also gives excellent results for certain superconductors, for example YBa2Cu3O7-δ. In all cases, the objective of a given method is to control the sizes of crystallites, specific surfaces and grain boundaries in order to best define superconducting properties. In this chapter, we present the results obtained by the different characterization techniques. The microstructural study was performed using a scanning electron microscope (SEM). The optical properties were performed using UV-Visible spectroscopy.

3. Doping elements

Doping is the most effective way to understand the mechanism responsible for the appearance of superconductivity. Quite often, the influence of impurities on superconductors is used as an effective probe of their physical properties. The use of substitutions is therefore one of the keys to understanding superconductivity. However, the effect of these substitutions on the critical temperature can or may not be correlated with their effect on other properties of the material. Generally, substitution by atoms, of different valence or atomic radius, results in a modification of doping, and structure in the immediate environment of the substituted site. In table 1 recapitulate the characteristics doping elements.

Table3.1: Doping elements

Compound	Defenition	Chemicale formula	Molar mass	Density	Melting point	Solubility
Nickel oxide	**Nickel(II) oxide is a black ionic chemical compound having in principle a nickel cation for an oxide or oxygen anion, of the formula NiO.**	**NiO**	**74,6928 g/mol**	**6,67 g/cm³**	**984 °C**	**In the water at zero degrees.**

3.1. Base Matrix Bi2212

In order to obtain Bi2212, a solid-solid reaction is required between the compounds described in the following table (table 3.2) under stochometric conditions. The formation of Bi 2212 passes through 3 stapes as the following:

The first stape: Bismuth oxide Bi_2O_3 reacts with CuO copper oxide to form the compound Bi_2CuO_4 according to the equation:

$$Bi_2O_3 + CuO \rightarrow Bi_2CuO_4 \quad .$$

The second stape: The resulting Bi_2CuO_4 reacts with calcium carbonate $CaCO_3$ to form a Phase encoded by the symbol A composed of elements Bi-Ca-Cu-O:

$$Bi_2CuO_4 + CaCO_3 \rightarrow Bi_2CaCuO_5 + CO_2.$$

The third stape: Phase A reacts with stronsium carbonate $SrCO_3$ to form Phase Bi2212.
The different information about the reactive compounds are presented in table 2

Table 3.2: Different information about the reactive compounds.

Compound	Dfenition	Chemical formula	Molar mass	Density	Melting point	Solubility
Bismuth oxide	Bismuth (III) oxide is an inorganic compound of bismuth and oxygen, with the formula bi_2o_3 and yellow in color. Arguably the most important bismuth compound industrially, it is often a starting point for bismuth chemistry.	Bi_2O_3	465.96 g/mol	8.9 g/cm^3	817 °C	insoluble in water; soluble in acidic medium
Strontium carbonate	Strontium carbonate is the carbonate salt of strontium. It comes in the form odourless white to grey powder. It is naturally present in the form of a mineral, strontianite.	$SrCO_3$	147.63 g/ mol	3.5 g/ cm^3	1497 °C	0.01 g/L (water, 20 °C)
Calcium carbonate	Calcium carbonate is composed of carbonate ions and calcium ions of white color. It is the major compound of limestones such as chalk, but also marble.	$CaCO_3$	100.0869 g / mol	2.71 g/ cm^3	825 °C	14mg/There 20 °C; zero; 0.013 g / L (at 25 °C),
Copper oxide	Copper oxide, is a compound of copper and oxygen, with the formula CuO. It is a black solid with an ionic structure, which melts at about 1200 °C by releasing some oxygen. Copper oxide exists in a natural form: tenorite.	CuO	79,545 g/mol	6,315 g/cm^3	1326 °C	In the water at zero degrees

3.2. Sample preparation procedure

3.2.1. The solid – solid reaction

This method, is the basis of powder metallurgy, it consists of the reaction of two or several phases at high temperature (an operation often called sintering), after many grindings. It is the method used in this work to prepare the doped powders of Bi2212 phase. The first step, consists in weighing the following base products : Bi_2O_3, $SrCO_3$, $CaCO_3$, CuO, NiO, La, Ba, then mixing them to obtain the stoichiometries of the different compositions (see figure 3.1) as presented in tables1-2 .

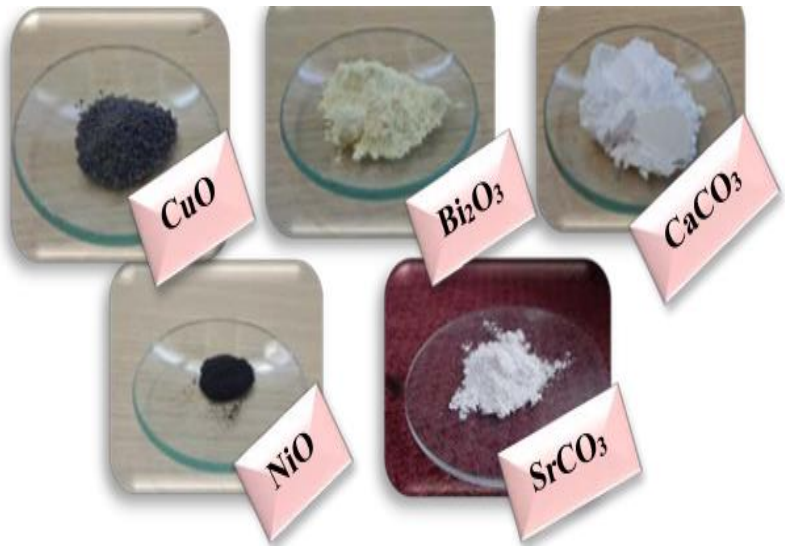

Figure3.1: different poders using in the solid –solid reaction

- **Calcule method**

We need 4 g from Bi2212 ($Bi_2Sr_2CaCu_2O_8$):

M_{Bi2212}= (2×208.980) + (2×87.620) + (40.073) +(2×63.546)+ (8×15.999)

M_{Bi2212}=888.357g/mol

M_{Bi2O3}= 465,957 g/mol m_{Bi2O3}= X g :

888.357g/mol → 4 g

465,957 g/mol → X g

X= (4×465,957)/ 888.357

X=2,0980g

Table 3.3: Quantities of basic products used.

Products	Bi_2O_3	$SrCO_3$	$CaCO_3$	CuO
M (g/mol)	465,957	147,628	100,988	79,545
m (g)	2,0980	1,3294	0,4506	0,7163

$m_{NiO\ 1\%} = 4 \times 1/100 = 0.04g$

Table 3.4: Quantities of NiO used.

NiO%	1%	3%	5%
m(g)	0.04	0.12	0.2

3.2.2. Mixing and grinding

The different products: Bi2O3, SrCO3, CaCO3, CuO, (NiO or La or Ba) are mixed, the mixture is then ground until a homogeneous powder is obtained. During the preparation of our samples grinding will be repeated several times in order to have a uniform distribution of the used products as it is showen in figure3.2.

mortar

Figure3.2: Mortar

3.2.3. Pastillage

After grinding the powder obtained will be compacted in the form of a pellet using a mold and a hydrostatic press.

3.2.4. Calcination

The purpose of this operation is to transform the powder mixture into a composition and crystal structure well defined, it consists in heating the mixture of starting products at high temperatures without reaching the melting state, moreover during from this step the carbonates of the mixture are removed in the form of CO_2 release (Figure 2.1). Carbonates decompose according to the following reactions:

$$SrCO_3 \rightarrow SrO + CO_2 \uparrow \quad , \quad CaCO_3 \rightarrow CaO + CO_2 \uparrow$$

In addition, the reaction between the different constituents is produced partially or totally during calcination; aggregates of small crystallites are then formed, which is very favorable for the second step of the synthesis.

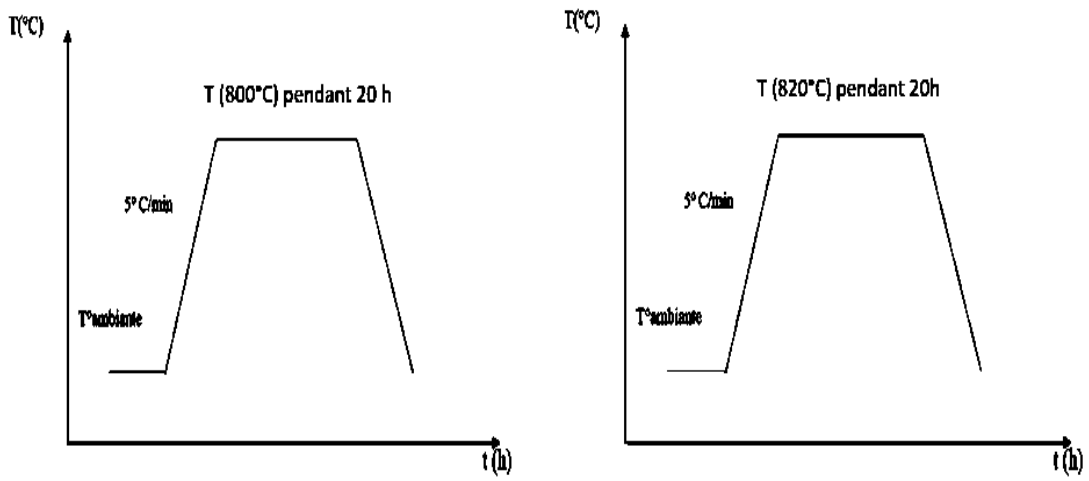

Figure 3.3: Thermal program of the calcination cycle

3.2.5. Formatting

After calcination our samples will be ground again and then compressed again times with a hydrostatic press to obtain cylindrical pellets of about 13 mm diameter and 1 to 5 mm thick. This makes it possible to bring the grains closer to the different phases and will thus allow an increase in the fraction of the desired phase.

mold

Figure3.4: a mold

3.2.6. Sintering

Sintering is a heat treatment performed at a temperature below the point of fusion of the main component of the material that allows the generation of strong bonds between particles by diffusion of matter. In most cases, sintering is accompanied by a shrinkage (reduction of the dimensions of the part) and therefore densification (reduction of volume of the room). The sintering cycle generally includes a heating period at the sintering temperature, then an isothermal period and finally a cooling. There heating speed should be controlled to prevent cracking, especially in materials ceramic. The isothermal bearing allows the growth of interarticular bonds and the densification of the material and sometimes results in grain magnification [1]. Sintering therefore corresponds to a transfer of matter, which takes place via a diffusion of atoms in the solid.

It has three effects:

- Consolidation of the material
- Densification by reducing porosity
- Grain growth

The sintering of our samples was carried out at 84440°C for 30h and 850°C for 60h. thermal cycle for sintering our samples is shown in Figure 3.5.

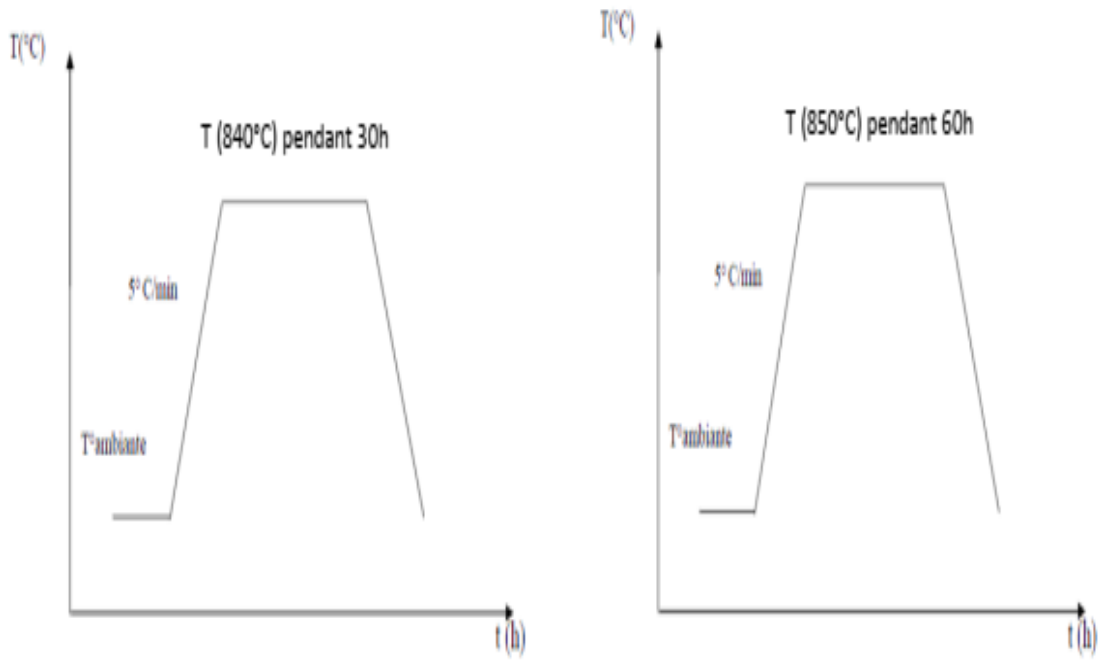

Figure 3.5: Thermal program of the sintering cycle.

Finally the prepering pellelt are presented in figure 3.6

pellet

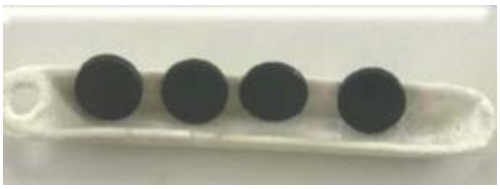

Figure3.6:Final pellet obtained

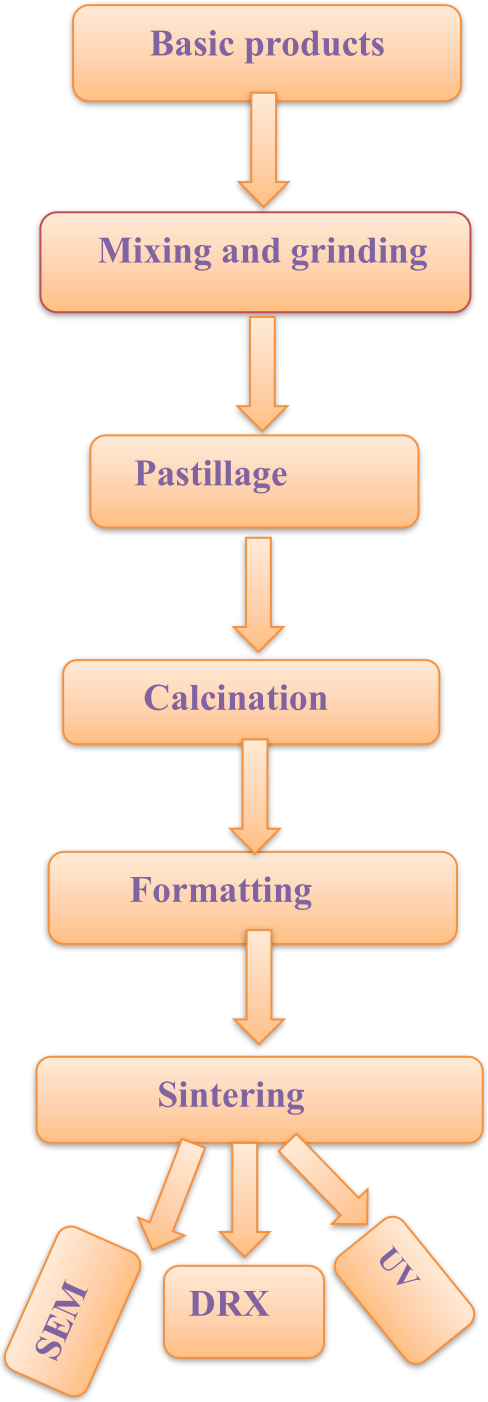

Fig3.7: Sample preparation process.

3.3. Techniques of Characterization

3.3.1.X-ray diffraction (XRD)

Figure 3.7-3.10 shows XRD spectra of the samples of Bi 2212, doped or not with Ni (x = 0;and 0.1). This figure illustrates the effect of Ni content x on obtaining phase Bi (Ni) 2212. We note the present of the main lines of the superconducting phase Bi2212 which vary depending on Nickel doping. The following remarks may be made :

Despite the majority presence of the Bi (Fe) 2212 phase, a number of secondary phases. The proportion of the phase Bi (Ni) 2223 decreases as a function of the Nickel concentration as it is presented in tables 3.5 and 3.6 The refinements of the cell parameters were carried out using the software MAUD (Materials Analysis Using Diffraction). The results give a tetragonal structure. The parameters obtained are reported in Tables 3.5 and 3.6 Figure 3.11 gives a representation of the variation of the cell parameter c as a function of the concentration x in Nikel. The value of c decreases approximately linearly.

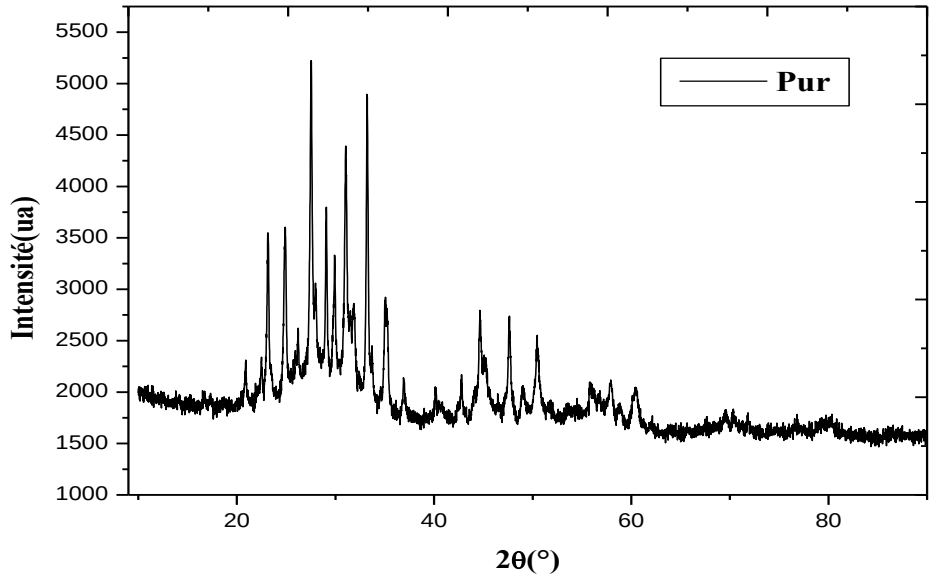

Figure.3.8: XRD diffractograms of Bi2Sr2CaCu2NixO8 + δ samples with or without Nickel

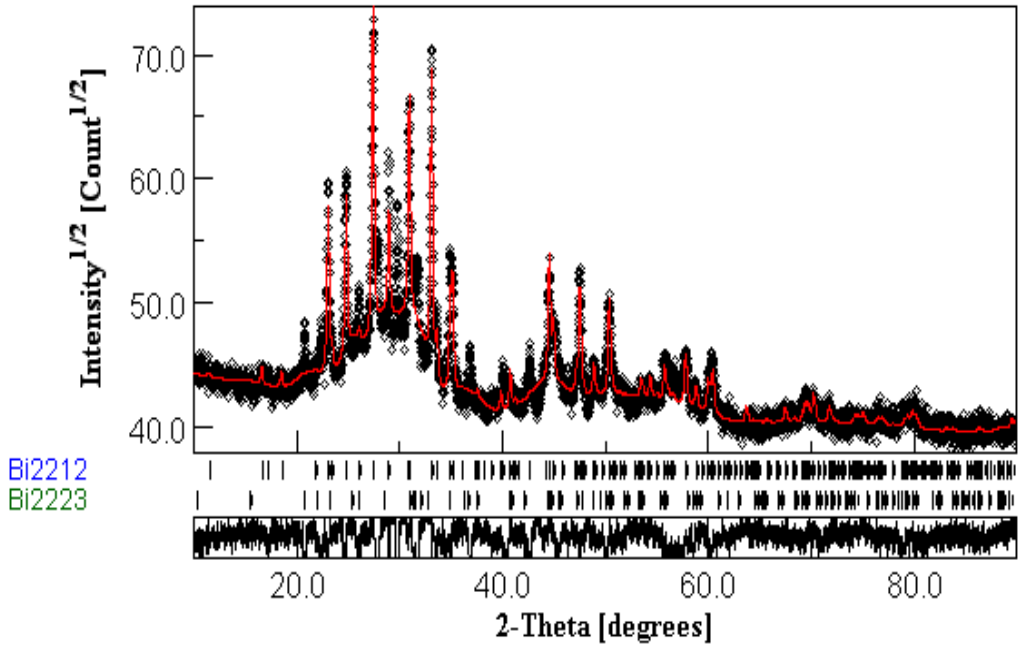

Figure.3.9: XRD diffractograms of Bi2Sr2CaCu2NixO8 + δ sample without Nickel

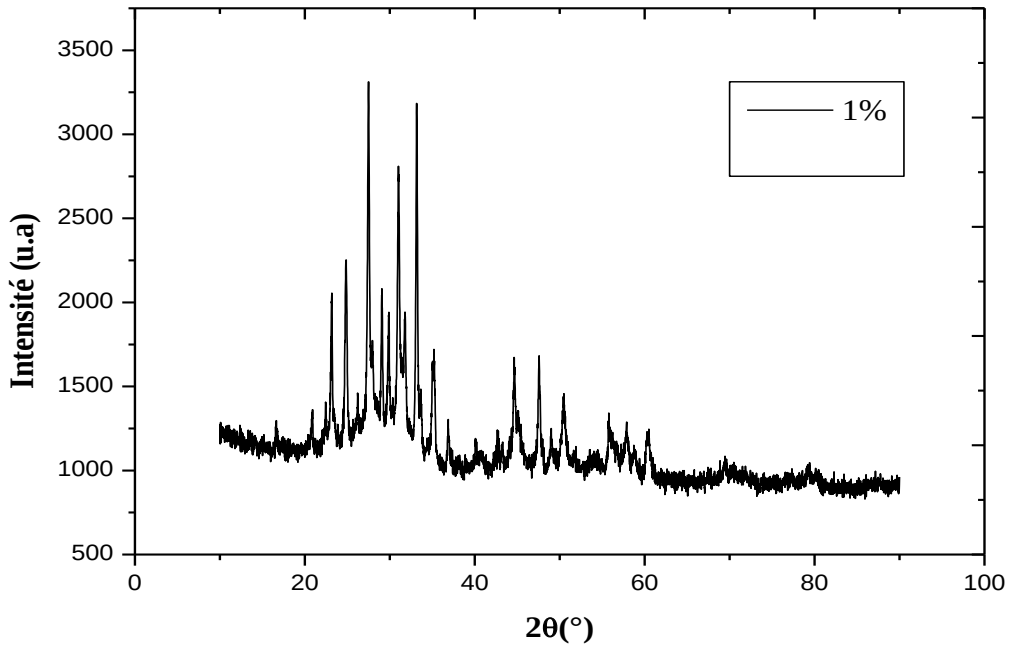

3

Figure.3.10: XRD diffractograms of Bi2Sr2CaCu2NixO8 + δ samples with 0.01 Nickel

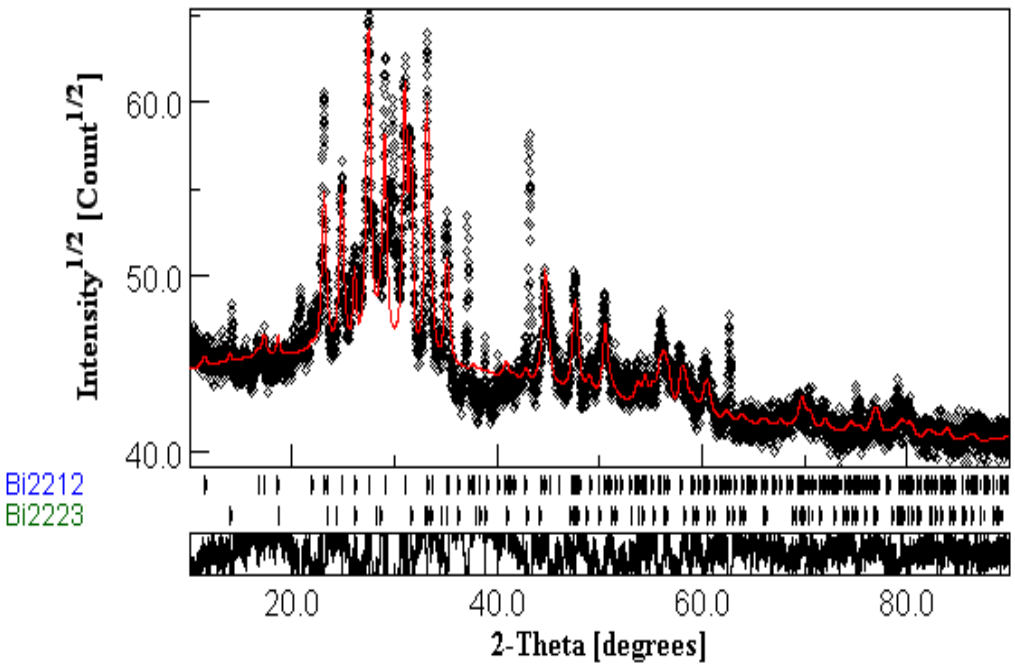

Figure.3.11: XRD diffractograms of Bi2Sr2CaCu2NixO8 + δ samples with 0.01 Nickel

Table 3.5: lattice parameters after refinement using MAUD program

Sample	a(Å)	b(Å)	c(Å)	Cristalllite Size (nm)	Microstrain Rate(%)
Pur	5,41077	5,40787	30,82893	81,35225	0.00071
1%	5,41006	5,40816	30,78025	79,12185	0.00577
5%	5,40280	5,39602	30,71253	25,6443	0,05112

Table 3.6: Showing the phases formed using MAUD program

Phase %	Bi2223	Error	Bi2212	Error
Pure	53,77643	±0,50685	49,5437	±0,75194
1%	49,77339	±1,96795	50,22661	±0,64415
5%	16,76259	±0,00547	83,23741	±2,27009

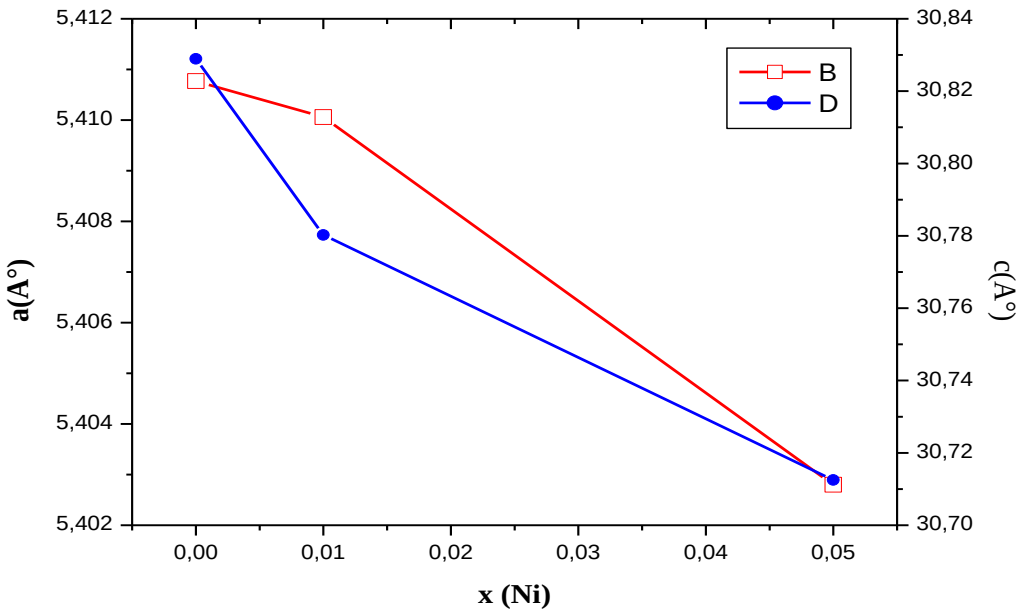

Figure.3.12: variation of x fonction of a and c parameters of Bi2Sr2CaCu2NixO8 + δ samples

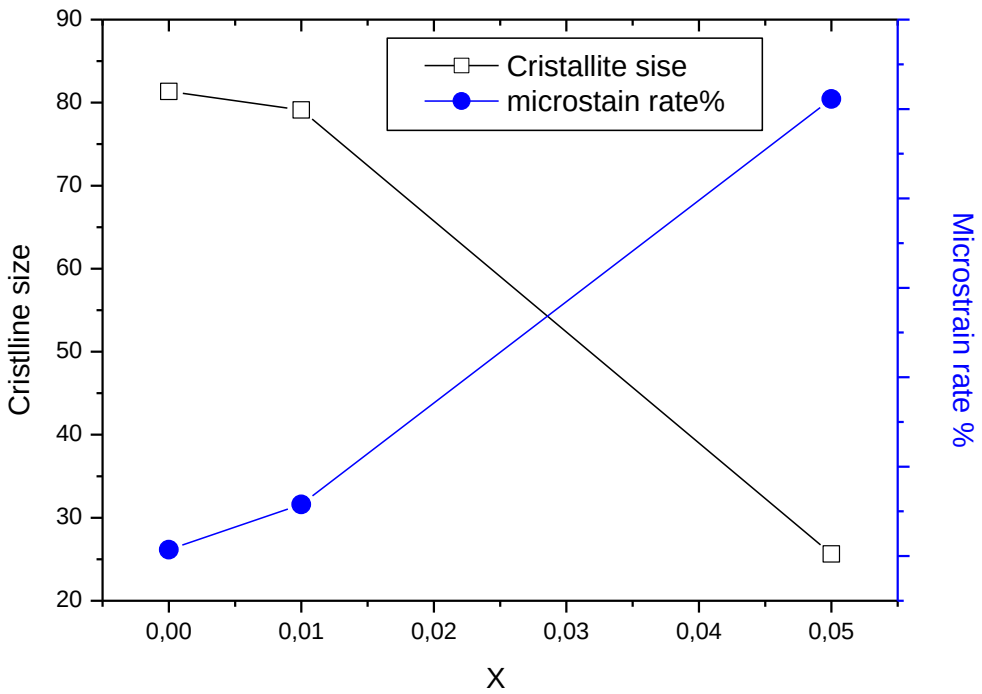

Figure.3.13: variation of x fonction of cristalline size znd microstarain rate % Bi2Sr2CaCu2NixO8 + δ samples

3.3.2. Study of the microstructure by SEM

The microstructure of the different samples is observed by scanning electron microscope (SEM). The SEM observations allow a qualitative and quantitative analysis of the samples produced. The qualitative analysis makes it possible to estimate the size and the morphology of the grains which are of great importance in the interpretation of the results of the physical measurements and in particular of the magnetization.

Figure 3.15 shows the SEM photomicrograph of the undoped (pure Bi2212) and doped samples with x = 0 and 0.01. The grains have the same morphology and the same alignment. The grain size has a random distribution with a few grains exceeding 5μm. The grains are quite dense and well connected. The shape of the grains is flattened (two-dimensional) characteristic of bismuth-based phases, with a size between 1 and 3 μm and the lamellar structure can be seen in all the samples. Some grains are inclined so to be confused with whiskers which are present for the sample having a x% of nickel equal to 0.01. Their growth can be from the liquid of the Bi2212 phase partially present [106]. The size of these grains is between 2 and 5μm. The increase in Ni level induces an increase in grain size.

In samples with x = 0.03 of Ni the grains are not clearly defined and a start of fusion seems to take place. This result is in agreement with the decrease in the intensities of the lines in the XRD spectrum of the sample with 0.03 Ni. These grains are denser, better connected with a much lower porosity than in the other samples. On the other hand, the orientation of the grains is very random. This is a confirmation of the rapid and disorderly growth of these same grains [128]. The incorporation of Nickel in the sample grains is confirmed by EDX.

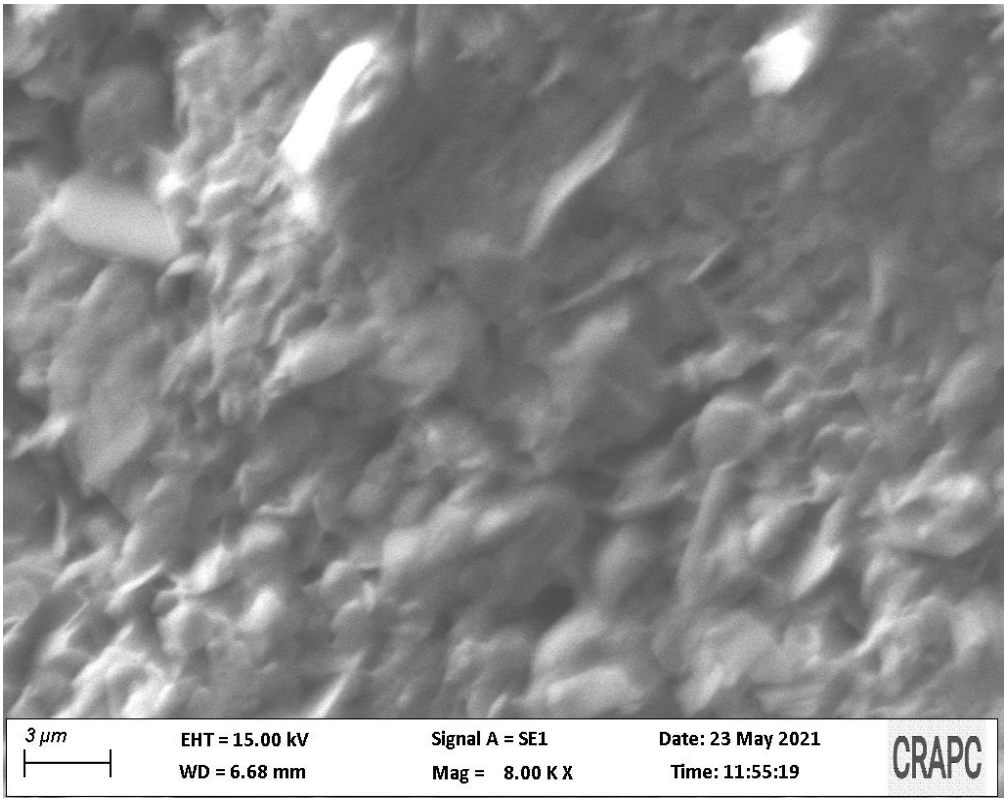

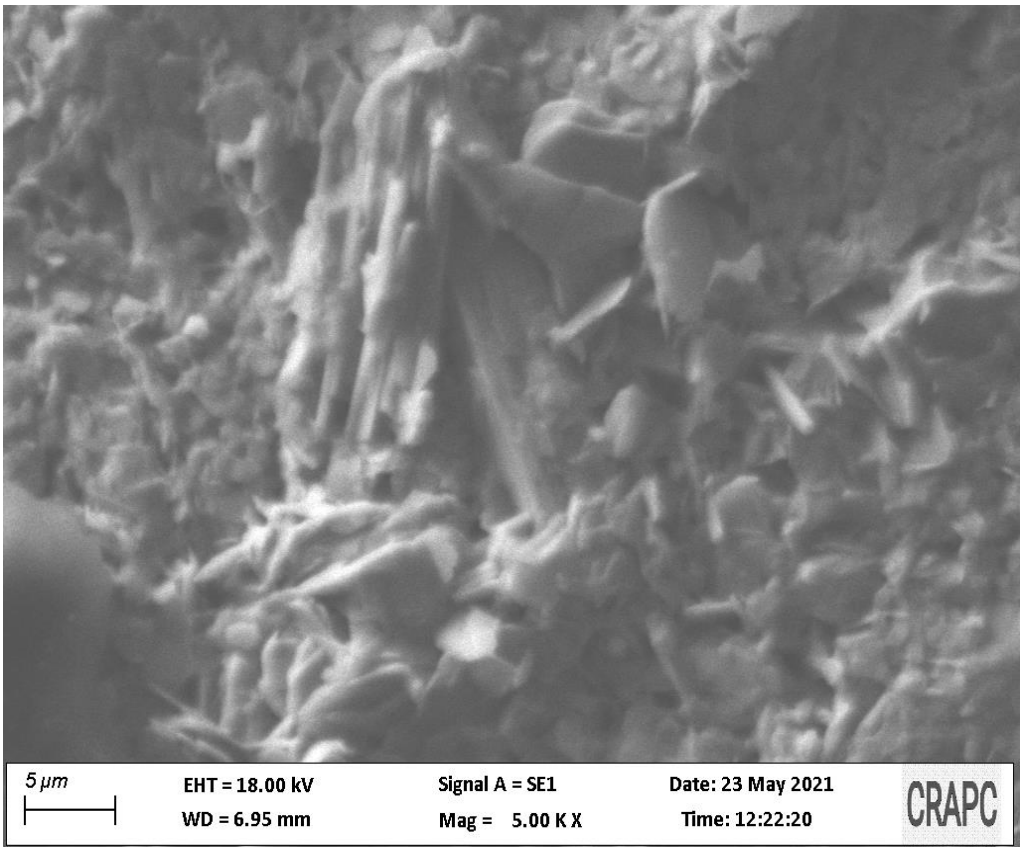

Figure 3.14: **SEM micrographs for the pure sample and doped with 1% Ni**

3.3.3. EDX Analysis

Figures 3.15 -3.16 show the compositions of elements detected in the EDX spectra of samples with Ni with x = 0 and 0.01 respectively

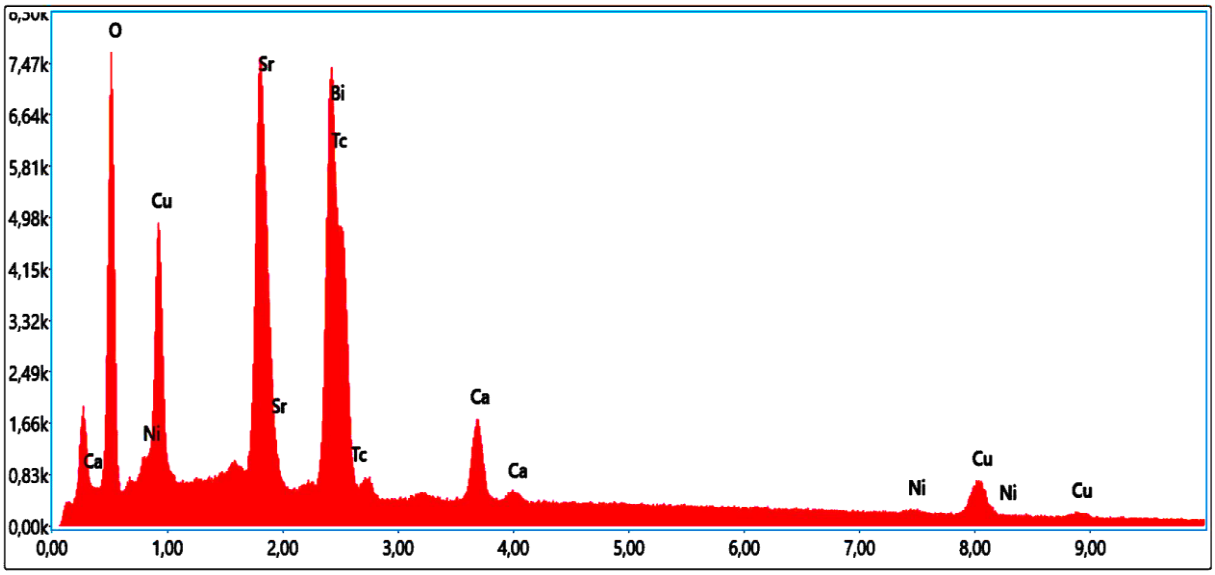

Figure 3.15: EDX spectrum of the sample supplemented with 0 Ni

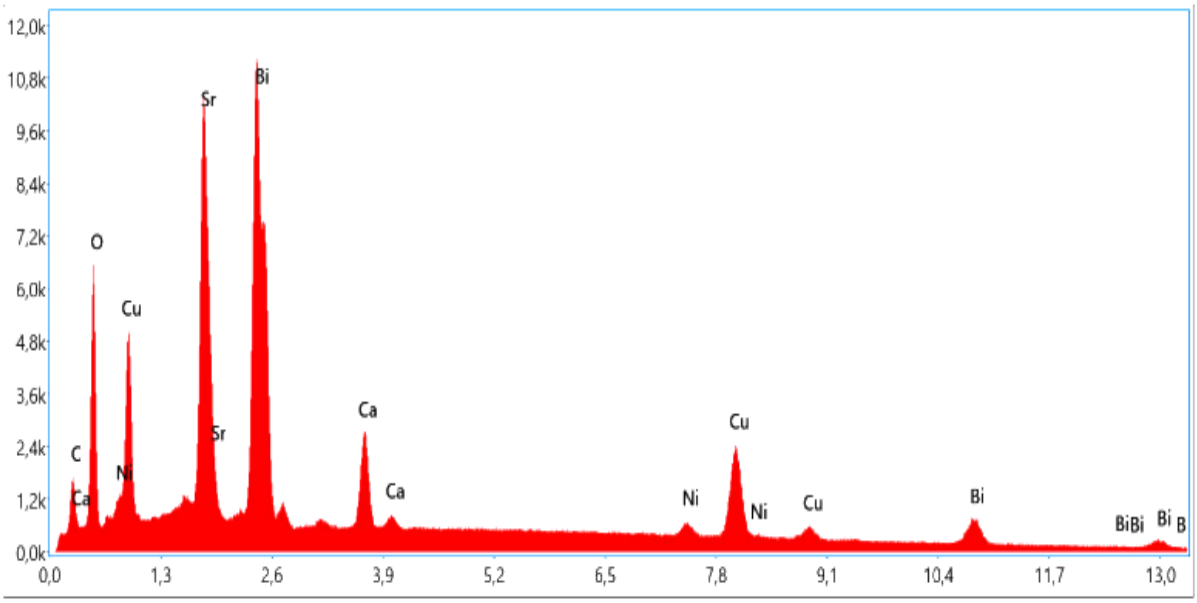

Figure 3.16: EDX spectrum of the sample supplemented with 0.01 Ni

The elements identified are bismuth (Bi), strontium (Sr), copper (Cu), oxygen (O), calcium (Ca), and Nickel (Ni). The table3.7 provided by the analysis instrument give the identified element, the concentration and the units for the concentration (Units column with wt% for percentage by mass).

Table 3.7: atomic percentages of simples

At.%	Pure	1%Ni
C	19.83	20.23
O	47.15	47.60
Bi	6.56	6.82
Cu	10.99	9.94
Sr	8.86	8.87
Ca	5.54	5.31
Ni	0	1.23

3.3.4. Optical characterizations

❖ UV-Visible

We can use optical measurements to determine the energy gap Eg in order to see how the energy gap values change by percentage and type of doping material, in addition to determining the type of transition . In UV spectrometry the energy gap can be deduced by he method of extrapolation from the variation of $(ah\nu)^{1/n}$ as a function of the energy of a photon $E = h\nu$.

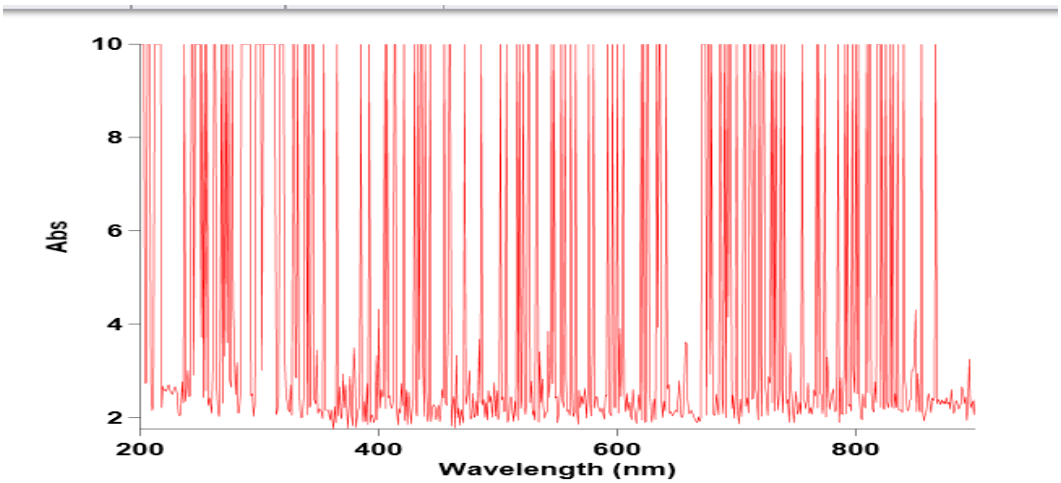

Figure.3.17: pure Bi2212 absorbance.

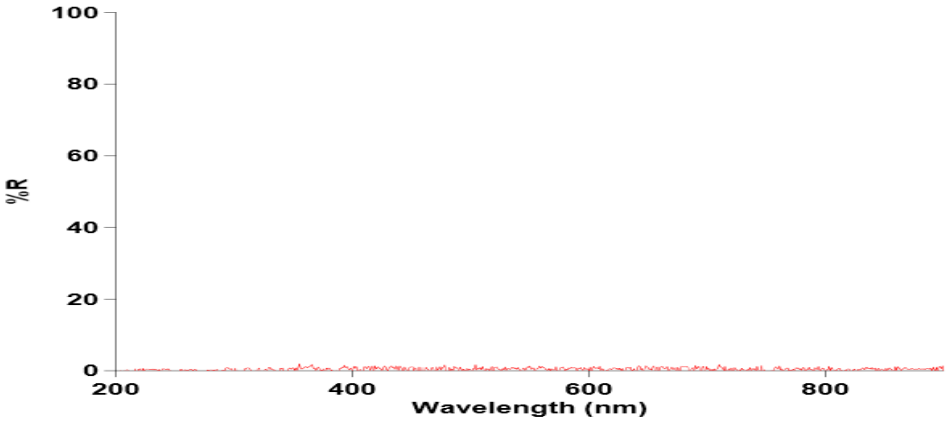

Figure3.18: pure Bi2212 refrectance.

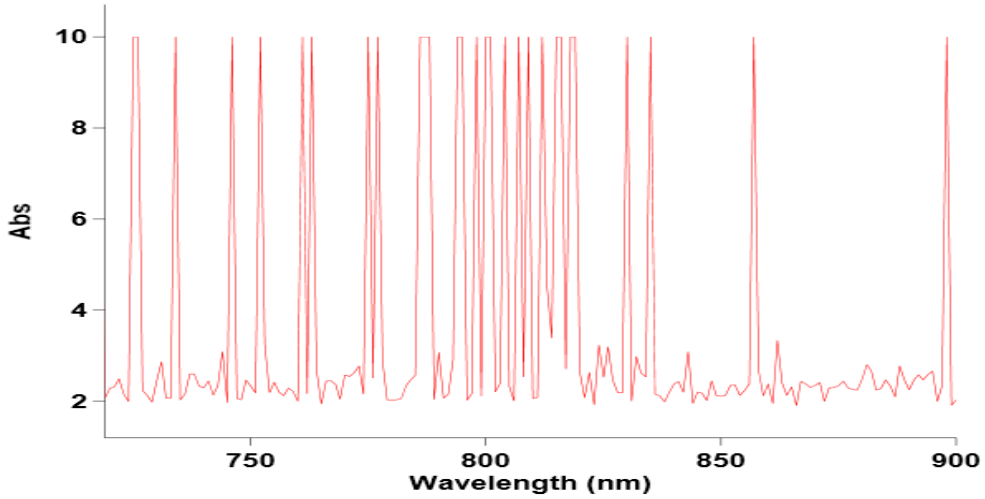

Figure.1.19: Bi2212 with 1% NiO absorbance.

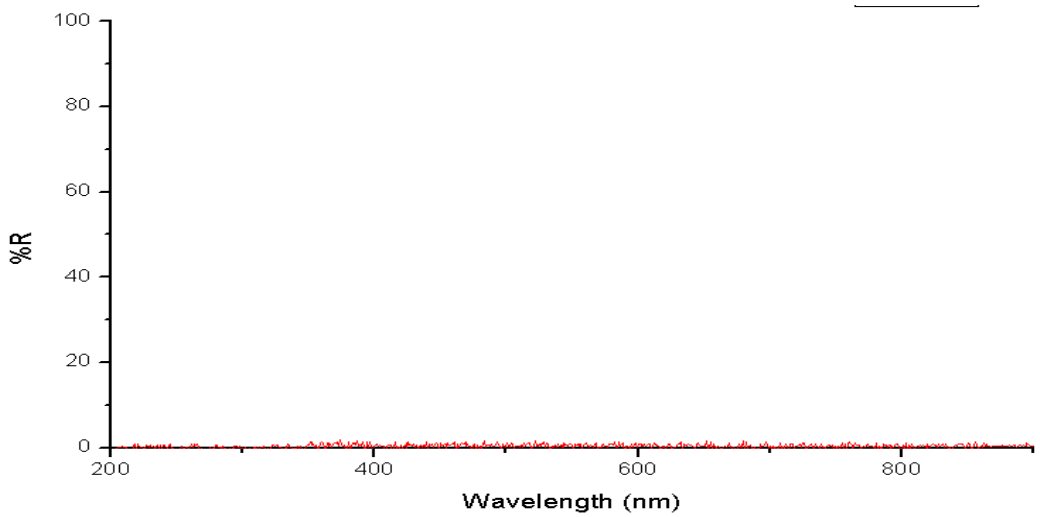

Figure.3.20: Bi2212 with 1% NiO refrectance.

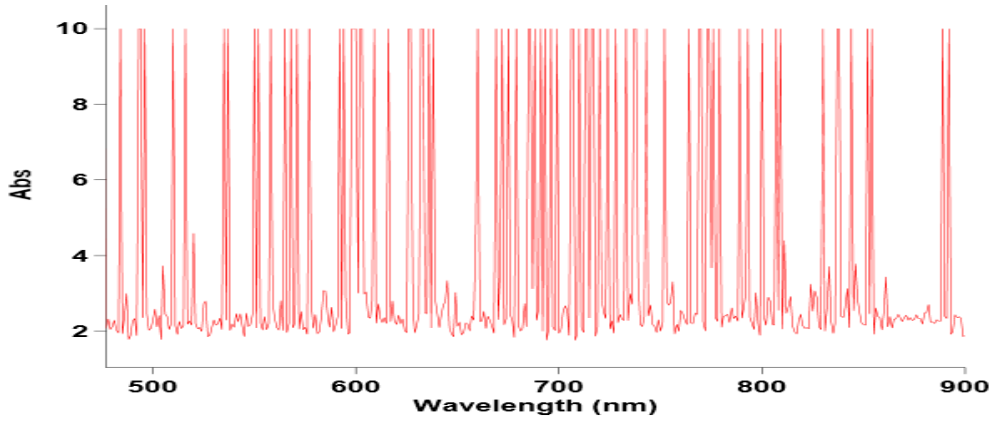

Figure.3.21: Bi2212 with 3% NiO absorbance.

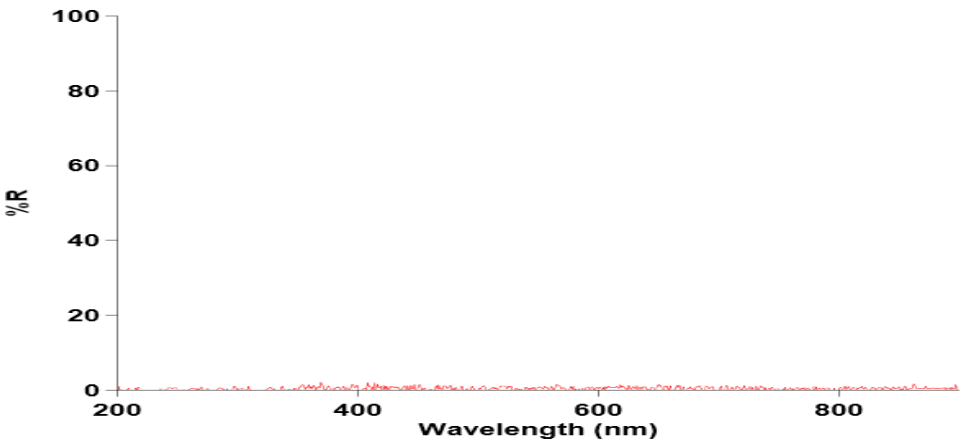

Figure.3.22: Bi2212 with 3% NiO refrectance.

- Absorbance

Figures 3.17, 3.19 and 3.21 such as absorption intensity as a function of the wavelength of pure Bi2212, Bi2212 with 1% NiO and Bi2212 with 3% NiO respectively.Reaching a wavelength of maximum absorption intensity indicates an electronic transition from a lower energy level to a higher energy level, observed in absorption figures increase in the number of wavelengths reaching maximum absorption intensity while corresponding to an increase in the percentage of doping since this indicates a decrease in the energy interval between levels, it is concluded that new energy levels have been created within the blocked package due to the dope called Fermi levels, which change the energy gap.

- Refrectance

Figures 3.18, 3.20 and 3.22 such as percentage of refrectance as a function of the wavelength of pure Bi2212, Bi2212 with 1% NiO and Bi2212 with3% NiO respectively.

An increase in the percentage of absorption and reflection is observed together with an increase in the percentage of doping, which indicates an increase in the opacity of the samples with an increase in the percentage of doping and thus a decrease in the percentage of transit because: $A + R + T = 1$ (3.1) A: absorption, R: reflection, T: transition

Reaching a wavelength of maximum absorption intensity indicates an electronic transition from a lower energy level to a higher energy level, observed in absorption figures increase in the number of wavelengths reaching maximum absorption intensity while corresponding to an increase in the percentage of doping since this indicates a decrease in the energy interval between levels, it is concluded that new energy levels have been created within the blocked package due to the dope called Fermi levels, which reduce the energy gap.

Optical gap determination:

In order to find out how the energy gap of the samples changes, the following Tauc formula is used :

$$\alpha h\nu = A\,(h\nu - E_g)^n \qquad (3.2)$$

A: is a constant reflecting the degree of disorder of the amorphous solid structure

h: is a White constant.

ν: is the wave frequency.

Eg: is the optical gap.

n: equal to 1/2 for the allowed electronic transitions of the direct gap.

$$\alpha h\nu = A\,(h\nu - E_g)^n \qquad (3.2)$$

$$\Rightarrow \quad \mathbf{(\alpha h\nu)^2 = A\,(h\nu - E_g)} \qquad (3.4)$$

α: absorption coefficient**:** $\boldsymbol{k = \frac{\alpha\lambda}{4\pi}}$ (3.5) $\Rightarrow \boldsymbol{\alpha = \frac{4\pi * k}{\lambda}}$ (3.6)

By plotting the product $(\alpha h\nu)^2$ as a f unction of (E= hν), and extrapolating in the linear area of the curve to $(\alpha h\nu)^2 = 0$. The value of the energy gap is the point of intersection of the line with the axis of the spacers (E=hν).

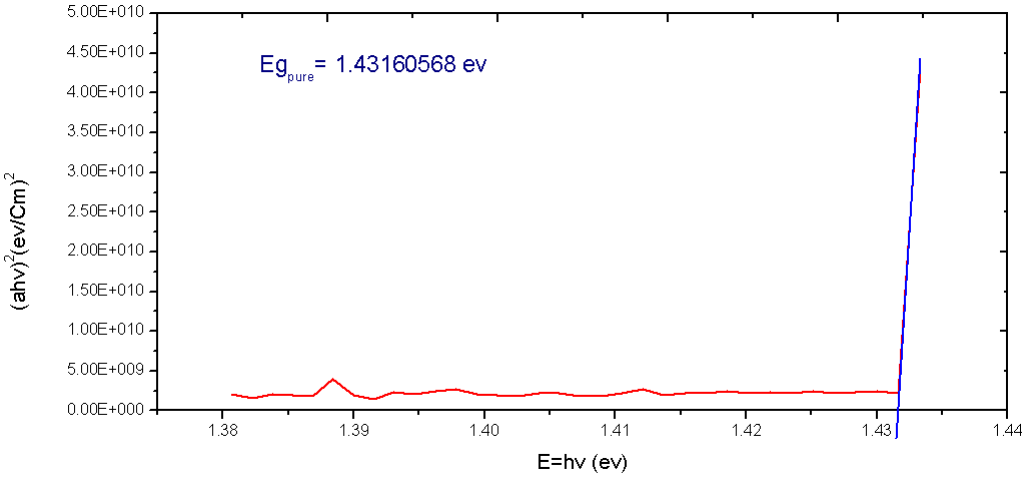

Figure.3.23: Enery gap calculation for x= 0.00

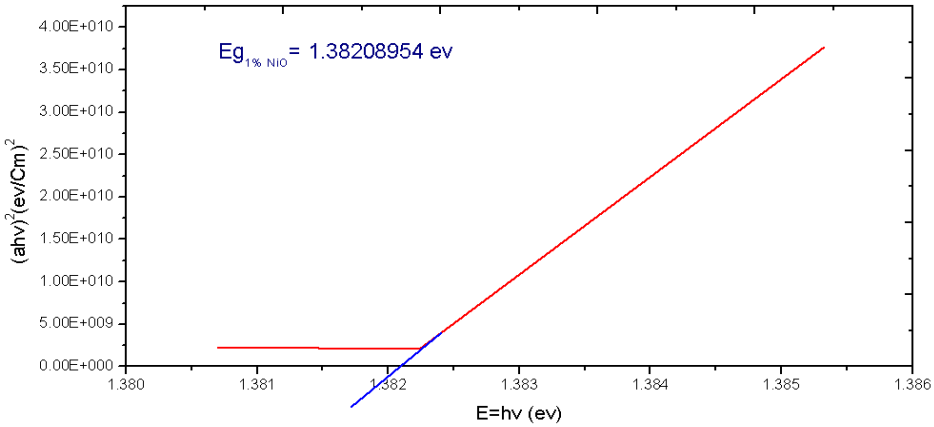

Figure.3.24:E nergy gap calculation for x=0.01

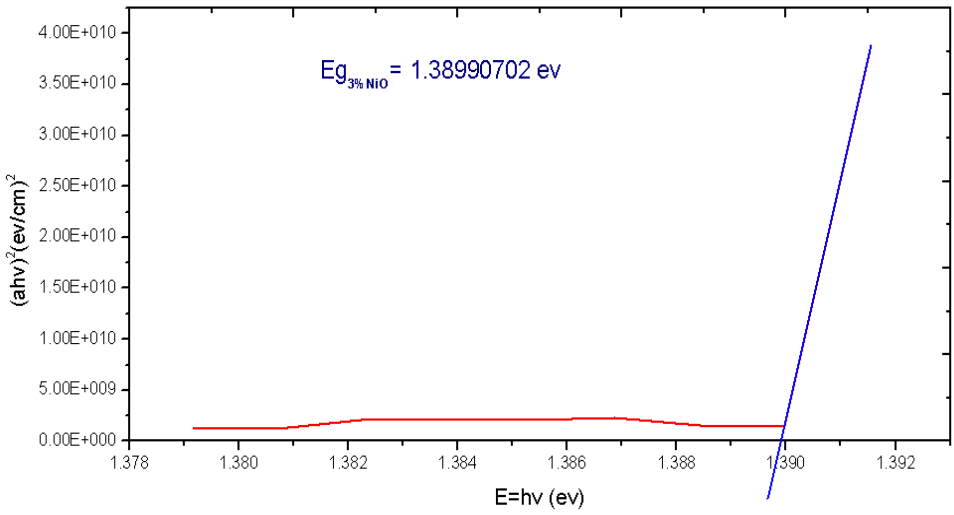

Figure.3.25:E nergy gap calculation for x=0.03

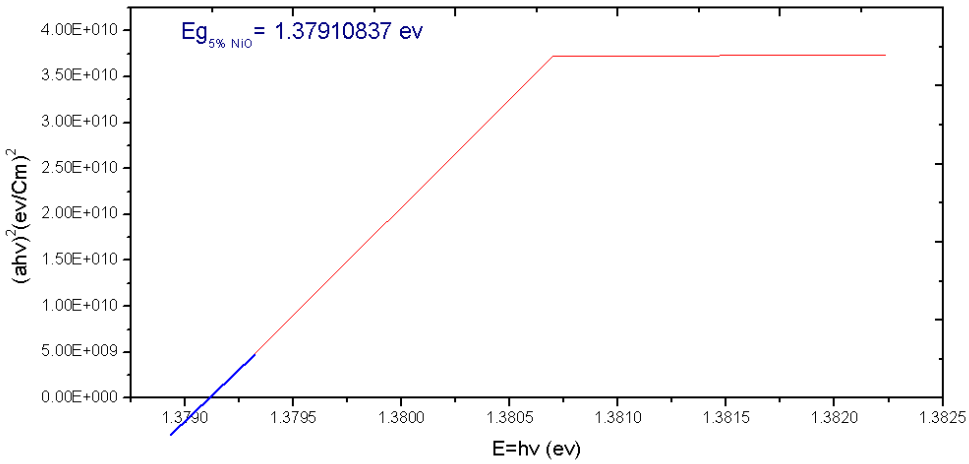

Figure.3.26 :E nergy gap calculation for x=0.05

One can see that the the band gap is overlapping the aforesaid region. Even though UV-Visible spectra are not essential for the superconducting material, it has been done to understand the underlying techniques of spectroscopy and analysis.

Conclusion

General conclusion

In this work we attended phase Bi2212, which belongs to high temperature superconductors ,ceramic type doping with nickel oxide (NiO) in different amounts 1%, 3% and 5% based on oxides: Bi_2O_3, $SrCO_3$, $CaCO_3$ and CuO , the samples prepared using X-ray diffraction method ,scanning electron microscope and ultraviolet ray for structural and optical study.

The results of our analysis:

- From XRD caracterization :

Refinement of X-ray diffraction (XRD) was carried out by material analysis using diffraction (MAUD) program to obtain the structural parameters such as lattice parameters, site occupancy of different atoms and orthorhombicity value for the all samples. Results show that NiO doping does not change the structure.

- From scanning electron microscopy:

The scanning electron microscopy (SEM) images of the samples show better grain connections by NiO doping.

- From UV visible spectrometer:

The energy gap is so small, from the order of 10^{-2} or 10^{-3}, that it can not appear in the spectrometer.

The UV-Vis spectra show the sample to be conducting at room temperature with no band gap present at 300K.

Future prospects:

We also have doping with Ba and La due to time constraints we weren't able to complete the work and we can also doping with (Ba, La, Sm, Pd, Pb, Fe, Zr, Mg, Ag).And the study of magnetic properties IRM, and electrical properties by studying the change of resistivity by the function of temperature.